Table 2. Echocardiographic Parameters in WT and CHOP-Deficient Mice at 4 and 8 Weeks After Sham Operation or TAC

	WT			$CHOP^{-/-}$		
Parameters	Sham (n=8)	TAC at 4 wk (n=8)	TAC at 8 wk (n=4)	Sham (n=6)	TAC at 4 wk (n=9)	TAC at 8 wk (n=3)
LVDd, mm	2.79±0.06	3.48±0.06*	4.38±0.52*	2.85±0.05	3.21±0.05*	3.67±0.24*‡
LVDs, mm	1.07±0.03	2.30±0.07*	3.50±0.68*	1.08±0.02	1.85±0.05*†	2.21±0.17*‡
LVPW, mm	0.64±0.02	0.88±0.02*	0.94±0.03*	0.64±0.03	0.80±0.02*†	0.87±0.04*
LVFS, %	60.7±1.1	35.0±1.0*	22.3±6.9*	62.2±0.9	42.6±1.1*†	39.8±0.8*‡
LVEF, %	91.4±0.6	63.4±2.7*	43.5±11.6*	91.8±0.5	74.6±1.1*†	71.2±1.2*‡
LV mass, mg	46.3±2.4	86.7±2.9*	111.8±7.5*	46.6±2.4	71.4±2.5*†	89.7±10.2*‡

LVDd indicates LV end-diastolic dimension; LVDs, LV end-systolic dimension; LVPW, LV posterior wall thickness; LVFS, LV fractional shortening; and LVEF, LV ejection fraction. Results are presented as mean±SEM.

*$P<0.05$ versus WT sham operation.

†$P<0.05$ versus WT TAC at 4 weeks.

‡$P<0.05$ versus WT TAC at 8 weeks.

Echocardiography revealed that the baseline left ventricular (LV) end-diastolic and systolic dimensions were not significantly different between WT mice and CHOP-deficient mice (Table 2). However, both the LV end-diastolic and end-systolic dimensions were significantly smaller in CHOP-deficient mice than in WT mice at 4 and 8 weeks after TAC (Table 2). Moreover, LV posterior wall thickness and calculated LV mass in CHOP-deficient mice were smaller than in WT mice. These findings suggest that CHOP plays an important role in the development of cardiac hypertrophy and failure by pressure overload in mice.

ER Stress Signaling in Pressure-Overloaded Hearts of WT and CHOP-Deficient Mice

Next, we investigated ER stress signaling in the pressure-overloaded hearts of WT mice and CHOP-deficient mice. We

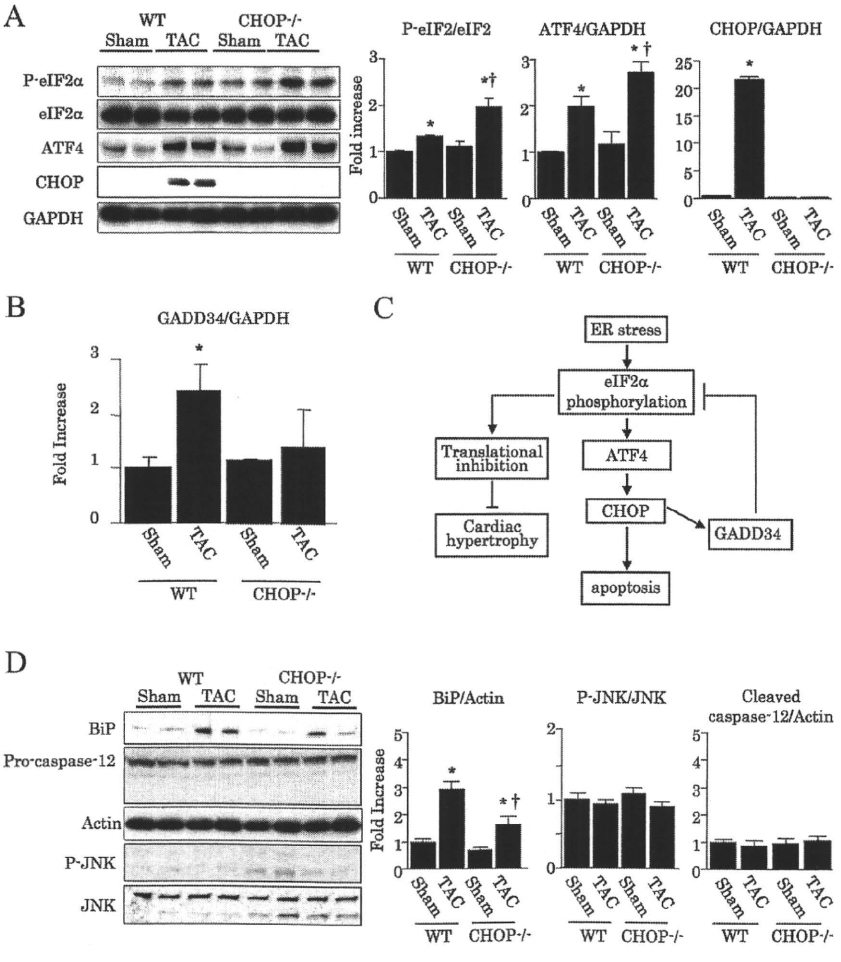

Figure 3. ER stress signaling in pressure-overloaded hearts of WT and CHOP-deficient mice. A, Representative immunoblotting (phospho [P-]-eIF2α, total eIF2α, ATF4, and GAPDH) of ER stress signaling in the hearts of WT and CHOP-deficient mice after sham or TAC operation. The intensity of bands for molecules involved in ER-initiated signaling was quantified from 3 independent experiments by densitometry. B, Quantitative real-time PCR analysis of GADD34 in the hearts of WT and CHOP-deficient mice after sham or TAC operation. C, Schematic diagram of CHOP ablation to attenuate cardiac hypertrophy and apoptosis. D, Representative immunoblotting analysis of ER-initiated apoptosis regulatory proteins in the hearts of WT and CHOP-deficient mice after sham or TAC operation. The intensity of bands for Bip and ER-initiated apoptosis regulatory proteins was quantified from 4 independent experiments by densitometry. Quantitative analysis showed the induction of BiP and CHOP but no increase in caspase-12 cleavage or JNK phosphorylation in the hearts of WT mice after TAC. Results are presented as mean±SEM. *†$P<0.05$ vs WT mice at 4 weeks after sham operation and TAC, respectively.

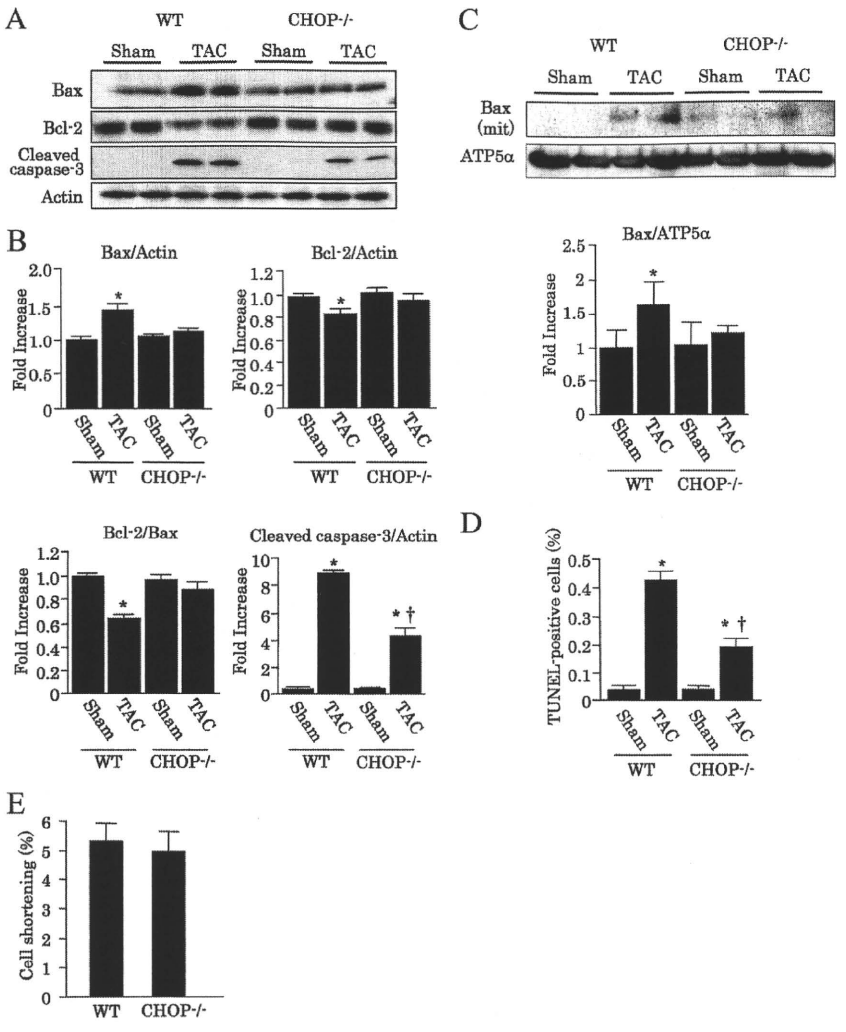

Figure 4. Bcl2 and Bax in pressure-overloaded hearts of WT and CHOP-deficient mice. A, Representative immunoblotting analysis of Bcl2 and Bax in the hearts of WT and CHOP-deficient mice. B, The intensity of bands was quantified from 4 independent experiments by densitometry. Bax protein levels were increased and Bcl2 protein levels were decreased by pressure overload in the hearts of WT mice, whereas Bax and Bcl2 protein levels were not significantly altered in CHOP-deficient mice. A decrease in the Bcl2/Bax ratio was seen in the hearts of WT mice but not CHOP-deficient mice as a result of pressure overload. The level of cleaved caspase-3 was significantly lower in the pressure-overloaded hearts of CHOP-deficient mice than in WT mice. C, Representative immunoblotting and quantitative analysis of mitochondrial Bax protein levels. Translocation of Bax to the mitochondria after TAC was significantly lower in CHOP-deficient mice than in WT mice. The intensity of bands was quantified from 4 independent experiments by densitometry. D, TUNEL staining of the hearts of WT (n=4) and CHOP-deficient (n=4) mice. TUNEL-positive cells were quantified by examination of 3000 nuclei from 10 randomly selected fields per heart. After TAC, the number of TUNEL-positive cells was significantly lower in CHOP-deficient mice than in WT mice. E, Cell shortening of isolated adult cardiomyocytes from WT and CHOP-deficient mice. Results are presented as mean±SEM. *†$P<0.05$ vs WT mice at 4 weeks after sham operation and TAC, respectively.

found that phosphorylation of eIF2α and expression of ATF4, either of which is an upstream signal of CHOP, were increased in hearts after TAC compared with those after sham operation in WT mice (Figure 3A). Expression of CHOP and its downstream target GADD34 was also increased by pressure overload in WT mice (Figure 3A and 3B). CHOP directly activates GADD34, which negatively regulates the phosphorylation of eIF2α and thus increases protein synthesis.[3,23,24] Consistently, in the hearts of CHOP-deficient mice, the increase in GADD34 caused by pressure overload was blunted, which led to enhanced phosphorylation of eIF2α and increased ATF4 (Figure 3A through 3C).

Among the factors involved in ER-initiated apoptotic signaling, caspase-12 or JNK was not activated by pressure overload in the hearts of WT and CHOP-deficient mice at 4 weeks after TAC (Figure 3D). This result was consistent with our previous findings.[9]

Bcl2 Family Genes in Sham-Operated and Pressure-Overloaded Hearts of WT and CHOP-Deficient Mice

The total Bax protein level was increased and the Bcl2 protein level was decreased in the pressure-overloaded hearts of WT mice, leading to a reduction in the Bcl2/Bax ratio (Figure 4A and 4B). We also observed an increase in Bax protein in the mitochondrial fraction from pressure-overloaded hearts of WT mice (Figure 4C). Furthermore, caspase-3 was activated and the number of TUNEL-positive cells was increased in pressure-overloaded hearts of WT mice (Figure 4A and 4D). In contrast, the levels of Bcl2, total Bax, and mitochondrial Bax protein in the hearts of CHOP-deficient mice with pressure overload did not differ from those in sham-operated mice (Figure 4A through 4C). The level of cleaved caspase-3 was lower and the number of TUNEL-positive cells was smaller in the hearts of CHOP-deficient mice with pressure overload compared with WT mice (Figure 4D). In the isolated adult cardiomyocyte from WT and CHOP-deficient mice, there were no significant differences in cardiac contractility under pacing conditions (Figure 4E and the online-only Data Supplement). These findings indicate that CHOP, a transcription factor involved in ER-initiated apoptotic signaling, has a role in mitochondria-dependent apoptosis in hearts subjected to pressure overload.

Finally, we assessed the role of CHOP in the expression of Bcl2 family genes in sham-operated and pressure-overloaded hearts from both WT and CHOP-deficient mice. In sham-operated hearts, none of the 15 Bcl2 family gene expressions showed differences between WT mice and CHOP-deficient mice (Table 3).

Table 3. Gene Expressions of Bcl2 Family Members in Hearts From WT and CHOP-Deficient Mice

	WT			CHOP$^{-/-}$		
Gene	Sham ($2^{-\Delta Ct}\times10^3$)	TAC ($2^{-\Delta Ct}\times10^3$)	TAC/Sham	Sham ($2^{-\Delta Ct}\times10^3$)	TAC ($2^{-\Delta Ct}\times10^3$)	TAC/Sham
Proapoptotic signaling						
Bad	14.3±0.5	15.9±0.1	1.1	15.1±0.2	15.6±1.7	1.0
Bak1	12.8±1.3	17.2±1.8	1.3	13.4±0.5	15.7±1.0	1.2
Bax	20.7±1.8	35.3±2.4	1.7*	22.3±1.2	25.5±1.1	1.1
Bid	0.5±0.0	1.0±0.1	2.0*	0.5±0.0	0.8±0.0	1.4*
Bnip3	264.4±71.2	233.1±10.7	0.9	218.7±20.9	264.2±33.1	1.2
Bnip3l	91.4±1.1	175.4±11.2	1.9*	108.9±10.4	100.6±11.2	0.9
Bok	11.6±0.3	15.0±1.4	1.3*	12.8±0.4	20.9±1.3	1.6*
Antiapoptotic signaling						
Bag1	353.4±36.6	327.5±63.3	0.9	389.7±36.2	456.1±36.8	1.2
Bag3	132.9±20.0	115.8±4.6	0.8	180.1±15.9	167.0±12.4	0.9
Bcl2	5.8±0.5	2.6±0.1	0.5*	5.2±0.2	6.9±1.3	1.3
Bcl2l1	15.0±0.4	10.1±0.8	0.7*	20.1±1.3	16.4±0.8	0.8
Bcl2l10	Undetected	Undetected	...	Undetected	Undetected	...
Bcl2l2	8.7±1.3	5.1±0.5	0.6*	6.3±0.8	4.4±0.4	0.7
Bnip2	60.7±6.2	70.5±5.2	1.2	71.2±1.9	67.8±4.5	1.0
Mcl1	179.6±6.3	276.1±16.2	1.5*	184.9±10.0	237.0±3.3	1.3*

Comprehensive analysis of the gene expressions of 15 Bcl2 family members in the sham-operated or pressure-overloaded hearts from WT and CHOP-deficient mice. Values are expressed as $2^{-\Delta Ct}\times10^3$, and data of sham-operated and pressure-overloaded hearts were analyzed with the $2^{-\Delta\Delta Ct}$ method. Results are presented as mean±SEM.

*$P<0.05$ versus gene expression at 4 weeks after sham operation on corresponding mice (n=3).

Consistent with the alterations in Bcl2 and Bax protein levels, we confirmed that *Bcl2* and *Bax* gene expressions decreased and increased in the pressure-overloaded hearts of WT mice, respectively (Table 3). In addition, we found significant changes in the expressions of other Bcl2 family member genes in pressure-overloaded hearts of WT mice compared with sham-operated ones: an increase in 3 proapoptotic genes (*Bid*, *Bnip3l*, and *Bok*) and 1 antiapoptotic gene (*Mcl1*) and a decrease in 2 antiapoptotic genes (*Bcl2l1* and *Bcl2l2*). In CHOP-deficient mice, except for *Bid*, *Bok*, and *Mcl1*, the expressions of Bcl2 family members did not change in pressure-overloaded hearts compared with sham-operated ones. Interestingly, in addition to *Bcl2* and *Bax*, the expressions of *Bnip3l*, *Bcl2l1*, and *Bcl2l2* in pressure-overloaded hearts differed between WT and CHOP-deficient mice. These findings suggest that ER-initiated apoptotic signaling via CHOP may mediate cardiac myocyte apoptosis by reducing the Bcl2/Bax ratio and/or by altering the expression of other members of the Bcl2 family to trigger mitochondria-initiated apoptosis.

Discussion

The present study confirmed an increase in the expression of BiP, an ER-resident chaperone that facilitates protein folding, in failing human hearts.[9] When ER stress is excessive and/or prolonged, apoptotic signals are initiated by the ER, including induction of CHOP, activation of JNK, and cleavage of caspase-12.[25–27] We confirmed that mRNA levels of ATF4 and CHOP were increased in failing human hearts, suggesting that CHOP could be important for proapoptotic signaling initiated by the ER in human heart failure. Experimental studies showed that CHOP has a critical role in dilated cardiomyopathy caused by aberrant ER quality control and in ischemic neuronal death,[28,29] suggesting that CHOP may be an important molecule in human heart and other diseases.

Therefore, we investigated the pathophysiological role of CHOP in the development of heart failure by using CHOP-deficient mice.[17] We previously demonstrated that cardiac dysfunction is induced in mice by pressure overload at 4 weeks after TAC.[9] Pressure overload caused by TAC increased the ratios of heart weight to body weight and of lung weight to body weight in WT mice, whereas these changes were partially but significantly attenuated in CHOP-deficient mice. In addition, histological analysis revealed that both cardiac hypertrophy and fibrosis in CHOP-deficient mice after TAC were significantly less compared with those in WT mice. Echocardiography demonstrated that LV enlargement and cardiac dysfunction after TAC were attenuated in CHOP-deficient mice compared with WT mice. In cultured rat neonatal cardiomyocytes, we found that the knockdown of CHOP blunted the increase in cell size in response to isoproterenol. These findings suggest that CHOP plays a crucial role in the development of cardiac hypertrophy and heart failure resulting from pressure overload.

CHOP regulates the expression of GADD34, which negatively regulates the phosphorylation of eIF2α. Enhanced phosphorylation of eIF2α reduces protein translation[30] and has been reported to mediate the inhibition of protein synthesis in the rat liver by vasopressin and the rat brain by essential amino acid deficiency.[31,32] Under CHOP-deficient conditions, decreased expression of GADD34 in pressure-overloaded hearts may lead to enhanced phosphorylation of eIF2α and

decreased protein synthesis. Thus, increased phosphorylation of eIF2α in hearts with pressure overload in CHOP-deficient mice is likely to contribute to the prevention of cardiac hypertrophy through the suppression of protein synthesis. Interestingly, pressure overload to hearts specifically activated CHOP but not caspase-12 or JNK. The promoter region of the CHOP gene contains binding sites for all of the major inducers of the unfolded protein response, including ATF4, ATF6, and XBP-1; these transcriptional factors are also involved in the induction of CHOP.[33] It will be important to clarify the selective activation of CHOP in future investigations.

Overexpression of CHOP leads to a decrease in Bcl2 protein, whereas overexpression of Bcl2 blocks CHOP-induced apoptosis.[12,34] In addition, overexpression of CHOP leads to translocation of Bax protein from the cytosol to the mitochondria.[35] Thus, the CHOP-mediated death signal is finally transmitted to the mitochondria, leading to activation of caspase-3.[27,36] In the present study, expression of Bax protein was increased and Bcl2 protein was decreased in the hearts of WT mice after TAC, consistent with previous data.[37] In contrast, these changes in apoptosis-regulating proteins did not occur in hearts of CHOP-deficient mice. These findings suggest that prolonged pressure overload leads to changes in apoptosis-regulating proteins via a CHOP-dependent pathway. Consequently, caspase-3 cleavage was reduced and the number of TUNEL-positive cells was smaller in the hearts of CHOP-deficient mice compared with WT mice at 4 weeks after TAC. Because there were no significant differences in contractility of isolated cardiomyocytes in WT and CHOP-deficient mice, it was likely that the improvement in cardiac function after TAC in CHOP-deficient mice was due to less apoptotic cell death.

Moreover, we performed real-time PCR microarray analysis for 15 Bcl2 family members. We found that the expressions of Bcl2 family member genes in sham-operated hearts were not significantly different between WT mice and CHOP-deficient mice. In pressure-overloaded hearts of WT mice, several Bcl2 family genes, including 4 proapoptotic genes and 4 antiapoptotic genes, were altered. Clarification of the role of each Bcl2 family gene in the development of heart failure is needed in our future studies. Interestingly, in addition to *Bcl2* and *Bax*, we found the difference in the expressions of 3 Bcl2 family genes in pressure-overloaded hearts between WT mice and CHOP-deficient mice: *Bnip3l*, *Bcl2l1*, and *Bcl2l2*. Bnip3l, also referred to as Nix, is induced in cardiac hypertrophy and mediates cardiomyocyte apoptosis.[38]

Consistent with this report, the increase in *Bnip3l* expression was blunted in pressure-overloaded hearts of CHOP-deficient mice. Furthermore, expressions of both *Bcl2l1* and *Bcl2l2* were decreased in pressure-overloaded hearts of WT but not CHOP-deficient mice. Bcl2l1 has been reported to be decreased in hypertrophic and failing hearts after pressure overload.[39] Although the role of Bcl2l2 in cardiomyocytes remains unclear, it is thought to play an important protective role in neurons and in the diseased brain.[40] Because the expressions of *Bid*, *Bok*, and *Mcl1* changed in a similar way between WT mice and CHOP-deficient mice, they may not contribute to the differences in cardiac dysfunction between WT mice and CHOP-deficient mice. These findings suggest that ER stress initiates CHOP-dependent apoptotic signaling, which finally leads to activation of mitochondria-dependent apoptotic signaling via several Bcl2 family members and contributes to heart failure induced by pressure overload. However, we need to carefully consider the difference in gene expression because of the small number of samples. Furthermore, because CHOP mediates apoptosis through the perturbation of the cellular redox state by depletion of intracellular glutathione and through protein-protein interactions,[35,41] we also need to consider whether CHOP influences mitochondria-independent apoptosis in failing hearts.

Conclusion

The present findings suggest that CHOP may be a logical target for the development of drugs to prevent cardiac hypertrophy and cardiomyocyte apoptosis in failing hearts.

Acknowledgment

We thank Dr Tomomi Gotoh (Kumamoto University, Kumamoto, Japan) for providing us with CHOP-deficient mice.

Sources of Funding

This study was supported by grants on Scientific Research from the Ministry of Education, Culture, Sports, Science, and Technology (No. 17590731) and a grant from the Japan Cardiovascular Research Foundation (No. 19390220).

Disclosures

None.

References

1. Ron D, Walter P. Signal integration in the endoplasmic reticulum unfolded protein response. *Nat Rev Mol Cell Biol.* 2007;8:519–529.
2. Xu C, Bailly-Maitre B, Reed JC. Endoplasmic reticulum stress: cell life and death decisions. *J Clin Invest.* 2005;115:2656–2664.
3. Marciniak SJ, Yun CY, Oyadomari S, Novoa I, Zhang Y, Jungreis R, Nagata K, Harding HP, Ron D. CHOP induces death by promoting protein synthesis and oxidation in the stressed endoplasmic reticulum. *Genes Dev.* 2004;18:3066–3077.
4. Urano F, Wang X, Bertolotti A, Zhang Y, Chung P, Harding HP, Ron D. Coupling of stress in the ER to activation of JNK protein kinases by transmembrane protein kinase IRE1. *Science.* 2000;287:664–666.
5. Szegezdi E, Fitzgerald U, Samali A. Caspase-12 and ER-stress-mediated apoptosis: the story so far. *Ann N Y Acad Sci.* 2003;1010:186–194.
6. Maron BJ, Ferrans VJ, Roberts WC. Ultrastructural features of degenerated cardiac muscle cells in patients with cardiac hypertrophy. *Am J Pathol.* 1975;79:387–434.
7. Kaufman RJ. Orchestrating the unfolded protein response in health and disease. *J Clin Invest.* 2002;110:1389–1398.
8. Shaffer AL, Shapiro-Shelef M, Iwakoshi NN, Lee AH, Qian SB, Zhao H, Yu X, Yang L, Tan BK, Rosenwald A, Hurt EM, Petroulakis E, Sonenberg N, Yewdell JW, Calame K, Glimcher LH, Staudt LM. XBP1, downstream of Blimp-1, expands the secretory apparatus and other organelles, and increases protein synthesis in plasma cell differentiation. *Immunity.* 2004;21:81–93.
9. Okada K, Minamino T, Tsukamoto Y, Liao Y, Tsukamoto O, Takashima S, Hirata A, Fujita M, Nagamachi Y, Nakatani T, Yutani C, Ozawa K, Ogawa S, Tomoike H, Hori M, Kitakaze M. Prolonged endoplasmic reticulum stress in hypertrophic and failing heart after aortic constriction: possible contribution of endoplasmic reticulum stress to cardiac myocyte apoptosis. *Circulation.* 2004;110:705–712.
10. Song B, Scheuner D, Ron D, Pennathur S, Kaufman RJ. Chop deletion reduces oxidative stress, improves beta cell function, and promotes cell survival in multiple mouse models of diabetes. *J Clin Invest.* 2008;118:3378–3389.
11. Silva RM, Ries V, Oo TF, Yarygina O, Jackson-Lewis V, Ryu EJ, Lu PD, Marciniak SJ, Ron D, Przedborski S, Kholodilov N, Greene LA, Burke RE. CHOP/GADD153 is a mediator of apoptotic death in substantia nigra

dopamine neurons in an in vivo neurotoxin model of parkinsonism. *J Neurochem.* 2005;95:974–986.
12. McCullough KD, Martindale JL, Klotz LO, Aw TY, Holbrook NJ. Gadd153 sensitizes cells to endoplasmic reticulum stress by down-regulating Bcl2 and perturbing the cellular redox state. *Mol Cell Biol.* 2001;21:1249–1259.
13. Jessup M, Brozena S. Heart failure. *N Engl J Med.* 2003;348:2007–2018.
14. Chien KR. Stress pathways and heart failure. *Cell.* 1999;98:555–558.
15. Foo RS, Mani K, Kitsis RN. Death begets failure in the heart. *J Clin Invest.* 2005;115:565–571.
16. MacLellan WR, Schneider MD. Death by design: programmed cell death in cardiovascular biology and disease. *Circ Res.* 1997;81:137–144.
17. Oyadomari S, Koizumi A, Takeda K, Gotoh T, Akira S, Araki E, Mori M. Targeted disruption of the Chop gene delays endoplasmic reticulum stress-mediated diabetes. *J Clin Invest.* 2002;109:525–532.
18. Liao Y, Takashima S, Zhao H, Asano Y, Shintani Y, Minamino T, Kim J, Fujita M, Hori M, Kitakaze M. Control of plasma glucose with alpha-glucosidase inhibitor attenuates oxidative stress and slows the progression of heart failure in mice. *Cardiovasc Res.* 2006;70:107–116.
19. Minamino T, Yujiri T, Terada N, Taffet GE, Michael LH, Johnson GL, Schneider MD. MEKK1 is essential for cardiac hypertrophy and dysfunction induced by Gq. *Proc Natl Acad Sci U S A.* 2002;99:3866–3871.
20. Fu HY, Minamino T, Tsukamoto O, Sawada T, Asai M, Kato H, Asano Y, Fujita M, Takashima S, Hori M, Kitakaze M. Overexpression of endoplasmic reticulum-resident chaperone attenuates cardiomyocyte death induced by proteasome inhibition. *Cardiovasc Res.* 2008;79:600–610.
21. Muraski JA, Fischer KM, Wu W, Cottage CT, Quijada P, Mason M, Din S, Gude N, Alvarez R Jr, Rota M, Kajstura J, Wang Z, Schaefer E, Chen X, MacDonnel S, Magnuson N, Houser SR, Anversa P, Sussman MA. Pim-1 kinase antagonizes aspects of myocardial hypertrophy and compensation to pathological pressure overload. *Proc Natl Acad Sci U S A.* 2008;105:13889–13894.
22. Livak KJ, Schmittgen TD. Analysis of relative gene expression data using real-time quantitative PCR and the 2(-Delta Delta C(T)) Method. *Methods.* 2001;25:402–408.
23. Novoa I, Zeng H, Harding HP, Ron D. Feedback inhibition of the unfolded protein response by GADD34-mediated dephosphorylation of eIF2alpha. *J Cell Biol.* 2001;153:1011–1022.
24. Zhang K, Kaufman RJ. The unfolded protein response: a stress signaling pathway critical for health and disease. *Neurology.* 2006;66:S102–S109.
25. Rasheva VI, Domingos PM. Cellular responses to endoplasmic reticulum stress and apoptosis. *Apoptosis.* 2009;14:996–1007.
26. Oyadomari S, Mori M. Roles of CHOP/GADD153 in endoplasmic reticulum stress. *Cell Death Differ.* 2004;11:381–389.
27. Zinszner H, Kuroda M, Wang X, Batchvarova N, Lightfoot RT, Remotti H, Stevens JL, Ron D. CHOP is implicated in programmed cell death in response to impaired function of the endoplasmic reticulum. *Genes Dev.* 1998;12:982–995.
28. Hamada H, Suzuki M, Yuasa S, Mimura N, Shinozuka N, Takada Y, Suzuki M, Nishino T, Nakaya H, Koseki H, Aoe T. Dilated cardiomyopathy caused by aberrant endoplasmic reticulum quality control in mutant KDEL receptor transgenic mice. *Mol Cell Biol.* 2004;24:8007–8017.
29. Tajiri S, Oyadomari S, Yano S, Morioka M, Gotoh T, Hamada JI, Ushio Y, Mori M. Ischemia-induced neuronal cell death is mediated by the endoplasmic reticulum stress pathway involving CHOP. *Cell Death Differ.* 2004;11:403–415.
30. Harding HP, Novoa I, Zhang Y, Zeng H, Wek R, Schapira M, Ron D. Regulated translation initiation controls stress-induced gene expression in mammalian cells. *Mol Cell.* 2000;6:1099–1108.
31. Kimball SR, Jefferson LS. Mechanism of the inhibition of protein synthesis by vasopressin in rat liver. *J Biol Chem.* 1990;265:16794–16798.
32. Gietzen DW, Ross CM, Hao S, Sharp JW. Phosphorylation of eIF2alpha is involved in the signaling of indispensable amino acid deficiency in the anterior piriform cortex of the brain in rats. *J Nutr.* 2004;134:717–723.
33. Yoshida H, Matsui T, Yamamoto A, Okada T, Mori K. XBP1 mRNA is induced by ATF6 and spliced by IRE1 in response to ER stress to produce a highly active transcription factor. *Cell.* 2001;107:881–891.
34. Matsumoto M, Minami M, Takeda K, Sakao Y, Akira S. Ectopic expression of CHOP (GADD153) induces apoptosis in M1 myeloblastic leukemia cells. *FEBS Lett.* 1996;395:143–147.
35. Gotoh T, Terada K, Oyadomari S, Mori M. hsp70-DnaJ chaperone pair prevents nitric oxide- and CHOP-induced apoptosis by inhibiting translocation of Bax to mitochondria. *Cell Death Differ.* 2004;11:390–402.
36. Breckenridge DG, Germain M, Mathai JP, Nguyen M, Shore GC. Regulation of apoptosis by endoplasmic reticulum pathways. *Oncogene.* 2003;22:8608–8618.
37. Condorelli G, Morisco C, Stassi G, Notte A, Farina F, Sgaramella G, de Rienzo A, Roncarati R, Trimarco B, Lembo G. Increased cardiomyocyte apoptosis and changes in proapoptotic and antiapoptotic genes bax and bcl-2 during left ventricular adaptations to chronic pressure overload in the rat. *Circulation.* 1999;99:3071–3078.
38. Yussman MG, Toyokawa T, Odley A, Lynch RA, Wu G, Colbert MC, Aronow BJ, Lorenz JN, Dorn GW, II. Mitochondrial death protein Nix is induced in cardiac hypertrophy and triggers apoptotic cardiomyopathy. *Nat Med.* 2002;8:725–730.
39. Sharma AK, Dhingra S, Khaper N, Singal PK. Activation of apoptotic processes during transition from hypertrophy to heart failure in guinea pigs. *Am J Physiol Heart Circ Physiol.* 2007;293:H1384–1390.
40. Zhu X, Wang Y, Ogawa O, Lee HG, Raina AK, Siedlak SL, Harris PL, Fujioka H, Shimohama S, Tabaton M, Atwood CS, Petersen RB, Perry G, Smith MA. Neuroprotective properties of Bcl-w in Alzheimer disease. *J Neurochem.* 2004;89:1233–1240.
41. Ron D, Habener JF. CHOP, a novel developmentally regulated nuclear protein that dimerizes with transcription factors C/EBP and LAP and functions as a dominant-negative inhibitor of gene transcription. *Genes Dev.* 1992;6:439–453.

CLINICAL PERSPECTIVE

Heart failure is a major and growing public health problem worldwide. Although cardiac hypertrophy is a risk factor for the development of heart failure, it is largely unknown how prolonged cardiac hypertrophy causes heart failure. Recently, accumulating evidence has demonstrated that a number of diseases, including neurodegenerative diseases and diabetes mellitus, are associated with the impairment of protein folding in the endoplasmic reticulum (ER). The ER responds to stress by upregulating ER chaperones or attenuating global protein synthesis, but prolonged and/or excess ER stress leads to apoptosis. Here, we provide evidence that C/EBP homologous protein (CHOP), a transcriptional factor that mediates ER-initiated apoptotic cell death, and the ER chaperone were elevated in human failing heart samples, suggesting that ER stress is induced human failing hearts. Pressure overload induced cardiac hypertrophy and failure, along with increased expression in the ER chaperone and CHOP in mice heart. Interestingly, CHOP-deficient mice showed less cardiac hypertrophy and better cardiac function after pressure overload. One possible mechanism for reduced cardiac hypertrophy was enhanced phosphorylation of eukaryotic translation initiation factor 2α, which reduces protein translation and is negatively regulated by CHOP, in pressure-overloaded hearts of CHOP-deficient mice. Furthermore, CHOP decreased Bcl2 protein levels and other Bcl2 family members in cardiomyocytes, suggesting that the ER-mitochondria pathway would play an important role in cell death in pressure-overloaded hearts. In conclusion, the present findings suggest that CHOP may be a logical target for development of drugs to prevent cardiac hypertrophy and cardiomyocyte cell death in failing hearts.

THE JOURNAL OF BIOLOGICAL CHEMISTRY VOL. 285, NO. 41, pp. 31337–31347, October 8, 2010

Isoform-specific Intermolecular Disulfide Bond Formation of Heterochromatin Protein 1 (HP1)*[S]

Received for publication, June 19, 2010, and in revised form, July 26, 2010 Published, JBC Papers in Press, August 1, 2010, DOI 10.1074/jbc.M110.155788

Shuichiro Higo[‡], Yoshihiro Asano[‡§¶], Hisakazu Kato[§], Satoru Yamazaki[¶], Atsushi Nakano[‡], Osamu Tsukamoto[¶], Osamu Seguchi[¶], Mitsutoshi Asai[‡], Masanori Asakura[¶], Hiroshi Asanuma[¶], Shoji Sanada[‡], Tetsuo Minamino[‡], Issei Komuro[‡], Masafumi Kitakaze[¶], and Seiji Takashima[‡§1]

From the Departments of [‡]Cardiovascular Medicine and [§]Molecular Cardiology, Osaka University Graduate School of Medicine, Suita, Osaka 565-0871 and the [¶]Department of Cardiovascular Medicine, National Cardiovascular Center, Suita, Osaka 565-8565, Japan

Three mammalian isoforms of heterochromatin protein 1 (HP1), α, β, and γ, play diverse roles in gene regulation. Despite their structural similarity, the diverse functions of these isoforms imply that they are additionally regulated by post-translational modifications. Here, we have identified intermolecular disulfide bond formation of HP1 cysteines in an isoform-specific manner. Cysteine 133 in HP1α and cysteine 177 in HP1γ were involved in intermolecular homodimerization. Although both HP1α and HP1γ contain reactive cysteine residues, only HP1γ readily and reversibly formed disulfide homodimers under oxidative conditions. Oxidatively dimerized HP1γ strongly and transiently interacted with TIF1β, a universal transcriptional co-repressor. Under oxidative conditions, HP1γ dimerized and held TIF1β in a chromatin component and inhibited its repression ability. Our results highlight a novel, isoform-specific role for HP1 as a sensor of the cellular redox state.

Heterochromatin protein 1 (HP1) was originally characterized as an abundant protein that binds pericentric heterochromatin (1). HP1 acts as a scaffold-like molecule, which is composed of two conserved domains as follows: the chromodomain (CD)[2] and the chromoshadow domain (CSD). The variable hinge region separates these two domains (2). The CD recognizes methylated lysine 9 of histone H3 (H3K9), which recruits HP1 to specific sites within the genome (3–5). The CSD promotes HP1 homodimer formation and provides a surface for interaction with a variety of other chromatin proteins (6, 7). Although genetic experiments previously revealed that HP1 works as a repressor of gene activation by propagation of a heterochromatin structure, emerging evidence has elucidated its diverse functions other than gene silencing (8). Some of these functions are regulated in an isoform-specific manner (9).

In vertebrates, three isoforms of HP1 exist as follows: α, β, and γ, all of which share highly conserved domains. Tethering any HP1 isoform upstream of a promoter equally triggers gene silencing concomitant with local chromatin condensation and an increase in H3K9 methylation (10–12), indicating their common silencing ability. However, nonredundant functions (13, 14), different binding affinities to other proteins (15–17) and different localizations in tissues (18, 19), of these three HP1 isoforms imply that α, β, and γ are functionally diverse. Furthermore, recent evidence clarified apparently opposite functions of HP1 isoforms, *e.g.* a role in transcriptional activation or in transcriptional elongation (20, 21). One mechanism that could account for such functional diversity of HP1 isoforms is post-translational modification, which could cause conformational changes in the molecule. In fact, reversible modifications of HP1 (*e.g.* phosphorylation) can modulate its function in response to various stimuli or cellular environments, suggesting an active role for HP1 beyond its known function as a marker of heterochromatin (17, 22). However, the precise modulatory mechanism across three HP1 isoforms that leads to functional differences remains to be elucidated.

Here, we identified isoform-specific disulfide bond formation as a novel post-translational modification of HP1. We analyzed the biochemical and functional characteristics of this oxidative modification. These data may offer a new insight into a novel role for HP1 during the cellular response to oxidative stress.

EXPERIMENTAL PROCEDURES

Materials—We used the following commercially available materials for Western blotting: anti-HP1α (H2164, Sigma; 19s2, Millipore); anti-HP1β (MAB3448, Chemicon); anti-HP1γ (42s2, Millipore); anti-FLAG M2-peroxidase antibody (Sigma); anti-histone H3 (ab1791, Abcam); anti-GAPDH (MAB374, Chemicon); and anti-TIF1β (4123, Cell Signaling). We also used anti-FLAG M2 affinity gel for immunoprecipitation. We used menadione (Sigma), H_2O_2 (Wako), and hydroxytamoxifen (4-OHT) (Sigma) for cell treatment.

Cell Fractionation—Cells were lysed with hypotonic lysis buffer (10 mM HEPES, pH 7.9, 1.5 mM $MgCl_2$, and 10 mM KCl) with 0.5% Nonidet P-40 and centrifuged at 20,000 × *g* for 5 min.

* This work was supported by grants-in-aid from the Ministry of Health, Labor, and Welfare of Japan, grants-in-aid from the Ministry of Education, Culture, Sports, Science, and Technology of Japan, grants from the Japan Heart Foundation, grants from the Japan Cardiovascular Research Foundation, a grant from the Japan Society for the Promotion of Science, Mochida Memorial Foundation for Medical and Pharmaceutical Research, Japan Medical Association, Japan Incurable Diseases Research Foundation, Osaka Medical Research Foundation for Incurable Diseases, Suzuken Memorial Foundation, and Japan China Medical Association.

[S] The on-line version of this article (available at http://www.jbc.org) contains supplemental Figs. S1–S4, "Experimental Procedures," and additional references.

[1] To whom correspondence should be addressed. Tel.: 81-6-6879-3472; Fax: 81-6-6879-3473; E-mail: takasima@medone.med.osaka-u.ac.jp.

[2] The abbreviations used are: CD, chromodomain; CSD, chromoshadow domain; HUVEC, human umbilical vein endothelial cell; 4-OHT, hydroxytamoxifen.

The supernatant was collected as the cytosolic fraction. Extraction buffer (20 mM HEPES, pH 7.9, 1.5 mM $MgCl_2$, 0.42 M NaCl, 0.2 mM EDTA, 25% glycerol) was added to the pellet, and ultrasonic agitation was performed (30-s sonication with 30-s interval, 4–6 times at 0 °C; Bioruptor, CosmoBio). The suspension was incubated for 15 min at 4 °C and centrifuged at 20,000 × *g* for 10 min. The supernatant was collected as the nuclear extract.

Column Chromatography—For anion exchange, whole cells were lysed with buffer A (20 mM Tris, pH 8.0, 5% acetonitrile) containing 5 mM EDTA and 1% Nonidet P-40 and incubated at 4 °C for 15 min. The lysate was centrifuged at 20,000 × *g* for 5 min, and the supernatant was filtered and loaded onto an anion-exchange column (Q-Sepharose High Performance, GE Healthcare) pre-equilibrated with buffer A. After unbound samples were washed, protein was eluted with a linear gradient (0–100%) of buffer B (buffer A with 1.0 M NaCl). For reverse-phase HPLC, purified protein samples and nuclear extracts were prepared with 0.3% trifluoroacetic acid (TFA) and 20% acetonitrile and applied to a phenyl reverse-phase column (4.6 × 250 mm; Nakalai Tesque). Bound proteins were eluted by a segmented linear gradient of increasing concentrations of buffer B (acetonitrile and 0.1% TFA) in buffer A (0.1% TFA) at a flow rate of 0.5 ml/min. Buffer B was increased at a rate of 1.0%/fraction (fast gradient) or 0.2%/fraction (slow gradient). Collected fractions were dried by a centrifugal evaporator and reconstituted with SDS sample buffer with or without 2.5% 2-mercaptoethanol (reducing or nonreducing conditions, respectively).

Triton Extraction—Triton extraction was carried out as described previously with modification (23). Cells were lysed with a hypotonic lysis buffer with 0.5% Nonidet P-40 and centrifuged at 20,000 × *g* for 5 min (as described above). The pellet was lysed in extraction buffer with 0.2% Triton X-100, incubated on ice for 30 min, and centrifuged at 20,000 × *g* for 5 min. The supernatant was kept as a Triton-soluble fraction. The remaining pellet was lysed in SDS sample buffer (250 mM Tris, 5% SDS, and 5% glycerol) with or without 2.5% 2-mercaptoethanol (reducing or nonreducing conditions, respectively), and ultrasonic agitation was performed as described above. After centrifugation at 20,000 × *g* for 5 min, the supernatant was kept as a Triton-insoluble fraction.

RNAi Knockdowns and Generation of HEK293T Stable Cells—Lentiviral particles derived from the pLKO.1-puro-containing shRNA sequence were purchased from the Mission shRNA library (Sigma). The oligonucleotide sequences of the shRNA were as follows: shRNA-6, CGACGTGTAGTGAATGGGAAA; and shRNA-7, GCGTTTCTTAACTCTCAGAAA. Lentiviral particles were used to transduce human umbilical vein endothelial cells (HUVECs) or HEK293T cells in the presence of 8 μg/ml Polybrene. To generate a HEK293T stable cell line, the infected cells were selected with 1 μg/ml puromycin. The stable cells in which HP1γ was almost completely depleted were next transfected with pEF-DEST51 HP1γ-FLAG WT or a C177S mutant (cloned from murine cDNA and resistant to shRNA), and the stable cells were selected with 5 μg/ml blasticidin.

GAL4-luciferase Reporter Assay—pC3-ERHBD-GAL4 or pC3-ERHBD-GAL4-KAP1 (TIF1β) with pGL4.31-PSV40-GAL4UAS were transfected using Lipofectamine 2000 into subconfluent HEK293T stable cells that were passaged 1 day before transfection. After 24 h, 0.04% ethanol or 4-OHT (500 nM) was added to the culture medium. Forty eight h after transfection, luciferase activity was measured by a luminometer (Lumat LB9507). Intranuclear mRNA levels of luciferase were measured as follows. Twenty four h after transfection, 4-OHT (500 nM) was added to the culture medium. Forty eight h after transfection, cells were lysed with a hypotonic lysis buffer with 0.5% Nonidet P-40 and centrifuged at 20,000 × *g* for 5 min (as described above). From the nuclear pellet, total RNA was isolated using RNA-Bee (Cosmo Bio). Total RNA was treated with DNase (Turbo DNA-free, Applied Biosystems) and was reverse-transcribed using a high capacity cDNA reverse transcription kit (Applied Biosystems). Luciferase mRNA levels were measured by real time quantitative PCR (SYBR Green ER, Invitrogen). Firefly luciferase cDNA was amplified using the following primers: 5′-TACCCACTCGAAGACGGGAC-3′ and 5′-ACTCGGCGTAGGTAATGTCCACCTC-3′. Human 18 S ribosomal RNA was measured using the following primers: 5′-GTAACCCGTTGAACCCCATT-3′ and 5′-CCATCCAATCGGTAGTAGCG-3′. The relative levels of luciferase mRNA were normalized to the mRNA levels of 18 S ribosomal RNA.

RESULTS

HP1α Forms Dimers via Disulfide Bonds through Cysteine 133—During purification of HP1α in our previous work (24), we found that endogenous HP1α separates into two peaks by fractionation using reverse-phase HPLC. To confirm this finding, we fractionated whole cell lysates from HEK293T cells using two-step column chromatography (Fig. 1*A*). Endogenous HP1α was eluted at a salt concentration ranging from 0.3 to 0.35 M on a Q-Sepharose anion-exchange column (Fig. 1*D*, *top panel*). We applied this single peak to a reverse-phase column. After elution with a fast gradient, HP1α was still detected as a single peak (Fig. 1*D*, *2nd panel*). However, when eluted with a slow gradient, HP1α separated into two peaks representing a hydrophilic and a hydrophobic form (Fig. 1*D*, *3rd panel*). Two other HP1α antibodies against different epitopes also detected both bands (data not shown), suggesting that these were biochemically different forms of HP1α. Even after direct fractionation of the nuclear extract, which includes the bulk of HP1α protein (Fig. 1*B*), endogenous HP1α showed a similar bimodal distribution (Fig. 1*D*, *4th panel*). In other primary cells (HUVECs, neonatal rat cardiomyocytes, and rat cardiac fibroblasts), similar bimodal peaks were observed (supplemental Fig. S1). In contrast, recombinant HP1α expressed in *Escherichia coli* (Fig. 1*C*) exhibited only one peak with elution characteristics similar to those of the hydrophilic peak under the same separating condition used for the endogenous protein (Fig. 1*D*, *bottom panel*). These data suggest that two different forms of HP1α endogenously exist in multiple cell types and that the late-eluted hydrophobic species may be a post-translationally modified form.

To further elucidate the molecular characteristics of these two forms of HP1α, we used recombinant FLAG-tagged HP1α (HP1α-FLAG). As with endogenous HP1α, HP1α-FLAG existed mainly as a nuclear protein (Fig. 1*E*) and exhibited the

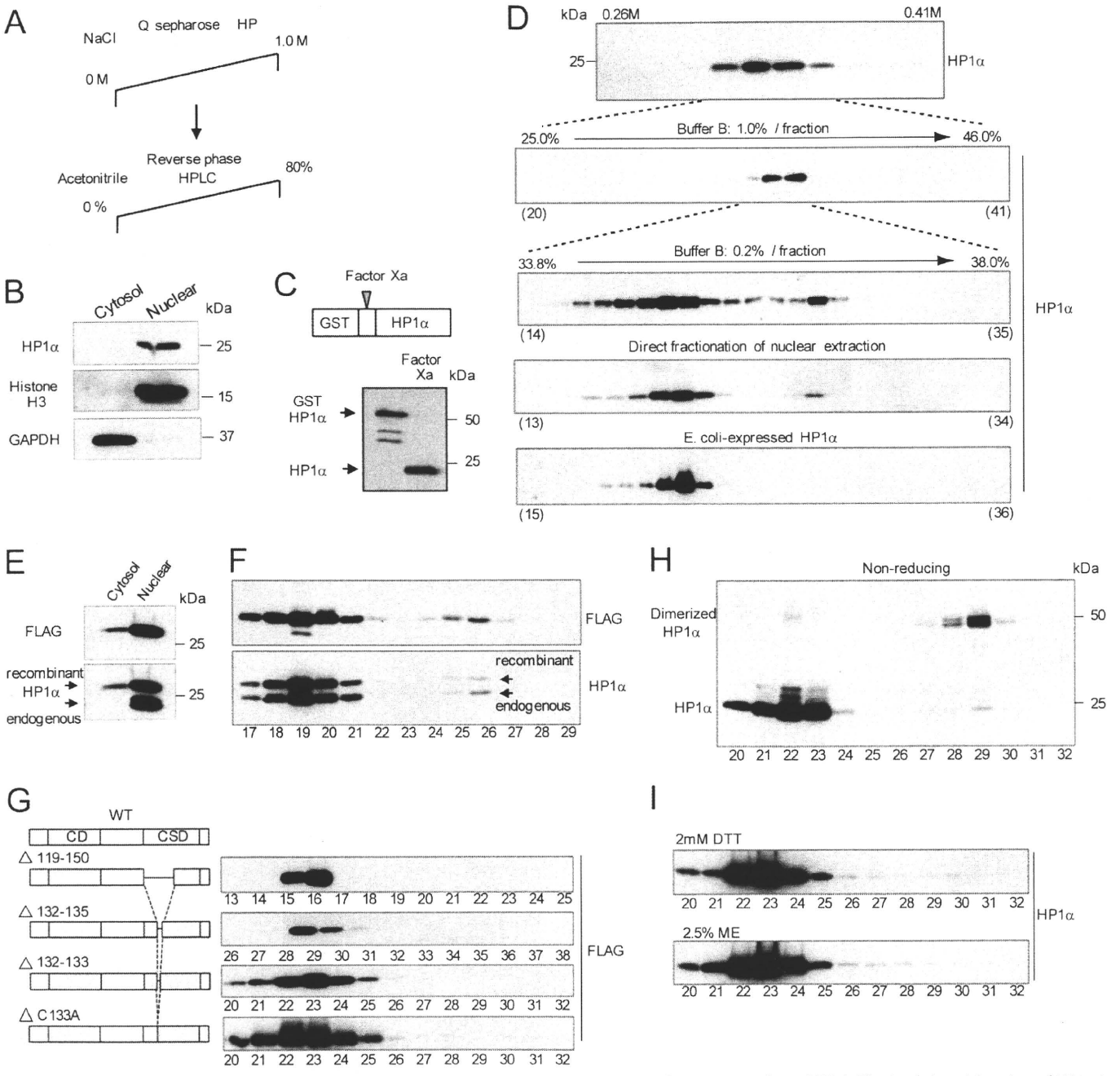

FIGURE 1. **Endogenous HP1α shows a bimodal distribution after protein purification by reverse-phase HPLC.** The late-eluted fraction of HP1α is oxidatively modified to form a disulfide bond. *A*, schematic representation of HP1α purification from cell lysates using sequential column chromatography. *B*, equal quantities of cytosolic and nuclear fractions from HEK293T cells were resolved by SDS-PAGE and probed with the indicated antibodies. *C*, GST-HP1α expressed in *E. coli* was purified and cleaved by Factor Xa (*upper panel*) and detected with anti-HP1α antibody (*lower panel*). *D*, HEK293T cell lysate was fractionated by a Q-Sepharose HP anion-exchange column. Eluted fractions were resolved by reducing SDS-PAGE and probed with anti-HP1α antibody (*top panel*). The *x* axis at the *upper edge* indicates salt concentration. HP1α fractions eluted from the anion-exchange column were next applied to a phenyl reverse-phase column. The fractions were eluted by a fast gradient (buffer B, 1.0% increase of acetonitrile concentration/fraction, *2nd panel from the top*) or by a slow gradient (buffer B, 0.2%/fraction, *3rd panel from the top*). Nuclear extraction from HEK293T cells (*4th panel from the top*) or HP1α purified from *E. coli* (*bottom panel*) was fractionated with the same slow gradient. The eluted fractions were resolved by reducing SDS-PAGE and probed with anti-HP1α antibody. *E*, equal quantities of cytosolic and nuclear fractions from HEK293T cells expressing HP1α-FLAG were resolved by SDS-PAGE and probed with the indicated antibodies. *F*, nuclear extract from HEK293T cells expressing HP1α-FLAG was directly applied to a reverse-phase column, and the eluted fractions were resolved by reducing SDS-PAGE and probed with the indicated antibodies. *G*, diagrams of the representative deletion mutant or point mutant of the HP1α protein during stepwise mutation analysis (*left column*). Nuclear extractions from HEK293T cells expressing each mutant protein were fractionated by reverse-phase HPLC, resolved by SDS-PAGE, and probed with anti-FLAG antibody (*right column*). *H*, endogenous HP1α was purified from the HEK293T cell lysate as shown in *A*. The fractions eluted from the reverse-phase column were resolved by SDS-PAGE under nonreducing conditions and probed with anti-HP1α antibody. *I*, nuclear extract from HEK293T cells was incubated with 2 mM DTT or 2.5% 2-mercaptoethanol (*ME*) for 30 min at 4 °C and then applied to a reverse-phase column. The eluted fractions were resolved by SDS-PAGE and probed with anti-HP1α antibody. *D* and *F–I*, the *x* axis at the *lower edge* indicates fraction numbers.

same bimodal distribution after reverse-phase HPLC (Fig. 1*F*). Thus, we concluded that HP1α-FLAG undergoes the same modification as endogenous HP1α, validating the use of the tagged protein for further analysis. Initially, we attempted to detect the specific modification directly by matrix-assisted laser desorption/ionization and time-of-flight mass spectrometry (MALDI-TOF/MS) (supplemental Fig. S2, *A–C*). Although we detected peptide masses from both fractions corresponding to ~75% of the entire HP1α sequence (supplemental Fig. S2*B*), we did not detect any distinct features in the mass spectra under two different digestion conditions (trypsin or Asp-N) (supplemental Fig. S2*C*). We next tried to detect a modified residue by making multiple, stepwise mutations throughout the entire HP1α molecule. We hypothesized that HP1α-FLAG lacking the modified residue would fractionate into a single peak by reverse-phase HPLC. First, we thoroughly screened the CD and hinge region, both of which are reported to be post-translationally modified (17, 22). However, we could not determine any specific amino acid residue from the mutational analysis (supplemental Fig. S2*D*). Second, we screened the CSD (supplemental Fig. S2*E*) and found that a deletion mutant lacking residues 119–150 (Δ119–150) was eluted as a single peak. We further narrowed down the deleted sequence 119–150 and finally found that a mutant in which cysteine 133 (Cys-133) was replaced by alanine (C133A) was eluted as a single peak (Fig. 1*G*). These data suggest that the single cysteine 133 residue is responsible for the separation of the hydrophobic fraction of HP1α.

Among post-translational modifications of cysteine, oxidation is a common feature. The thiol side chain can be oxidized to sulfenic acid (-SOH), sulfenyl amide (–SN), a disulfide bond (–SS–) or an irreversibly oxidized form (25). We examined the electrophoresis pattern of the two separated fractions of HP1α under nonreducing conditions and found that the hydrophobic form of HP1α shifted to a molecular weight twice its size, indicating that this HP1α formed a homodimer (Fig. 1*H*). In contrast, the mobility of the hydrophilic HP1α was unchanged. Because this dimer was nondissociable both under the strong acidic conditions of the reverse-phase HPLC and under the denaturing conditions during SDS-PAGE, it seemed to be linked by a covalent bond. Pretreatment with reducing agents, such as 2 mM DTT or 2.5% 2-mercaptoethanol, completely abolished the hydrophobic fraction (Fig. 1*I*). Taken together, these data suggest that endogenous HP1α dimerizes by intermolecular disulfide bond formation via Cys-133.

HP1α and HP1γ Both Possess an Isoform-specific Cysteine Residue for Disulfide Bond Formation—The sequence identity among the three HP1 isoforms is remarkably high (Fig. 2*A*), with up to 80% homology in the CSD. However, Cys-133 is specific to HP1α and is replaced by a serine in HP1β and HP1γ (highlighted in *red* in Fig. 2*A*). Therefore, we evaluated whether this oxidative modification was specific for HP1α. Endogenous HP1β was fractionated as a single peak by reverse-phase HPLC. However, endogenous HP1γ was isolated as two separate peaks (Fig. 2*B*). Both the hydrophilic and the hydrophobic fractions of HP1γ were eluted independently of those of HP1α suggesting that these two isoforms did not interact with each other during reverse-phase HPLC fractionation. Similar to HP1α, the hydrophobic form of HP1γ also dimerized (Fig. 2*C*). HP1β contains only two cysteines, both of which are conserved among the isoforms (Cys-59 and Cys-160 of HP1α; highlighted in *blue* in Fig. 2*A*). HP1γ has three cysteines, and one of the cysteines, Cys-177, is an isoform-specific residue located in the C terminus of the CSD. This residue is replaced by tyrosine in HP1α and HP1β (highlighted in *red* in Fig. 2*A*). Mutational analysis of these cysteine residues revealed that only isoform-specific Cys-133 of HP1α and Cys-177 of HP1γ were involved in dimerization (Fig. 2*D*). Mutating the corresponding residues of HP1β, Ser-129 (matched to Cys-133 of HP1α) or Tyr-173 (matched to Cys-177 of HP1γ), to cysteines created the late-eluted hydrophobic form (Fig. 2*E*). These hydrophobic forms of HP1β dimerized similarly with HP1α and HP1γ (Fig. 2*F*). The other two HP1β mutants, S141C and S162C, did not form disulfide bonds. Together, these data suggest that even though their overall structures are highly conserved, endogenous HP1α and HP1γ possess isoform-specific cysteine residues involved in the intermolecular disulfide bond formation. These two positions of the disulfide-linked cysteines are structurally sensitive to oxidation within the CSD.

HP1γ Is More Sensitive to Oxidation than HP1α in Vitro—We tested whether the differences in the positions of the modified cysteine residues between HP1α and HP1γ influenced their sensitivity to oxidation *in vitro*. Under mild oxidative conditions, only a low level of dimerized HP1α was detected even after a long exposure to air oxidation (Fig. 3*A*, *left panels*). In contrast, under the same conditions, HP1γ was easily oxidized to form disulfide bonds (Fig. 3*A*, *right panels*). Treatment with DTT reversed the disulfide formation of HP1γ. These data indicate that HP1γ is more sensitive to oxidation and more readily forms a disulfide dimer *in vitro*.

Using purified and oxidized HP1γ-FLAG, the intermolecular disulfide bond was confirmed by MALDI-TOF/MS analysis. The late-eluted dimerized fraction of HP1γ-FLAG was resolved by nonreducing SDS-PAGE, and the excised band was divided into two samples. One sample was reduced, carbamidomethylated with iodoacetamide, and digested by trypsin. The other sample was directly digested without pretreatment. The expected digested peptide, including Cys-177, consisted of the C terminus of HP1γ and lysine residue within the linker peptide (Fig. 3*B*). The mass spectrum peak of 3084.32, which was detected only in the nonreduced sample, corresponded to the estimated mass of the dimeric peptide connected by a disulfide bond via Cys-177 (3084.35) (Fig. 3*C*, *upper panel*). In contrast, the peak at 1600.68, which was detected only in the reduced sample, corresponded to the estimated mass of the monomeric peptide, including carbamidomethylated Cys-177 (1600.71) (Fig. 3*C*, *lower panel*). No other significant mass spectral peaks from the intermolecular disulfide bond were detected.

HP1γ, but Not HP1α, Readily Forms Disulfide Bonds under in Vivo Oxidative Conditions—We assessed whether this oxidative modification was promoted under *in vivo* oxidative conditions using a pro-oxidant agent, 2-methyl-1,4-naphthoquinone (menadione), which caused oxidative stress in cells (Fig. 4*A*) (26). Menadione treatment caused a dose- and time-dependent increase in the disulfide bond formation of HP1γ in COS7 cells (Fig. 4*B*, *left two panels*). The disulfide dimerization of HP1γ

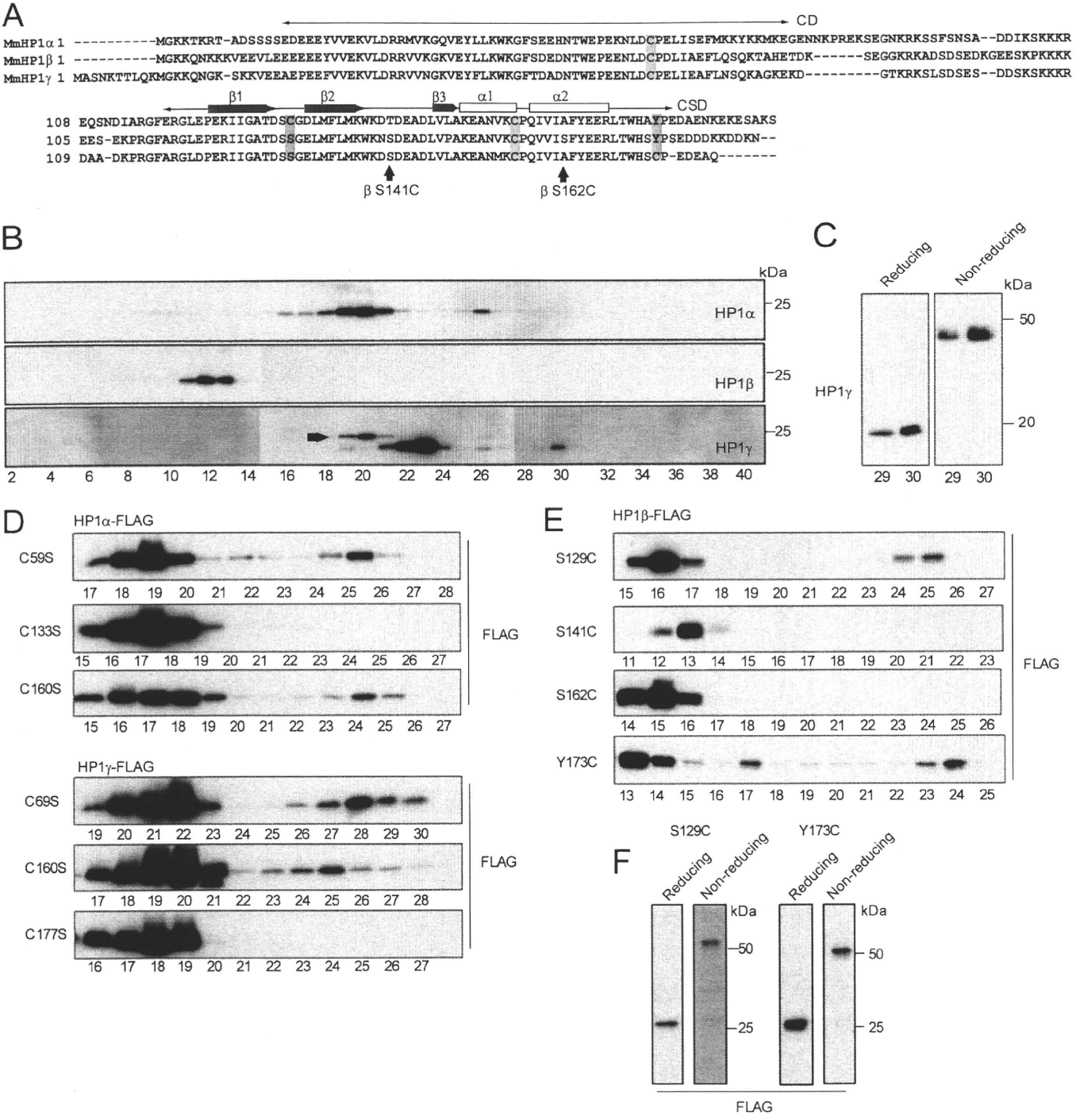

FIGURE 2. **Both HP1α and HP1γ possess isoform-specific cysteine residues that are oxidatively modified to form disulfide bonds.** *A*, amino acid sequence alignment among mouse HP1 isoforms. *Crosswise two-headed arrows* indicate the N-terminal CD and C-terminal CSD. The *bold blue arrow* and *bold white line* along the CSD indicate β-sheet and α-helix, respectively. *Blue highlights* represent the following: two cysteine residues conserved among the HP1 family (Cys-59 and Cys-160; HP1α). *Red highlights* represent the following: position of the cysteine residue specific to HP1α (Cys-133) or HP1γ (Cys-177). The *arrowhead* indicates the position of the mutated HP1β serine residue (shown in *E*). *B*, nuclear extract from HEK293T cells was directly applied to a reverse-phase column, and the eluted fractions were resolved by SDS-PAGE and probed with anti-HP1α, -β, or -γ antibodies. The immunoblotting procedure was performed by consecutive stripping and reprobing with each antibody of the same membrane. The *upper band* of fraction 20 in the *bottom panel* (*arrowhead*) indicates the residual signal from hydrophilic HP1α. *C*, hydrophobic fractions of HP1γ purified from HEK293T cells (as shown in Fig. 1*A*) were resolved by SDS-PAGE under reducing or nonreducing conditions and probed with anti-HP1γ antibody. *D*, nuclear extract from HEK293T cells expressing each HP1α-FLAG (*top three panels*) or HP1γ-FLAG (*bottom three panels*) with a cysteine-to-serine mutation was fractionated by reverse-phase HPLC, resolved by SDS-PAGE, and probed with anti-FLAG antibody. *E*, nuclear extract from HEK293T cells expressing HP1β-FLAG with each serine-to-cysteine or tyrosine-to-cysteine mutation was fractionated by reverse-phase HPLC, resolved by SDS-PAGE, and probed with anti-FLAG antibody. *F*, late-eluted hydrophobic fraction of the HP1β-FLAG mutant (S129C or Y173C) was resolved by reducing or nonreducing SDS-PAGE and probed with anti-FLAG antibody. *B–E*, the *x* axis at the lower edge indicates fraction numbers.

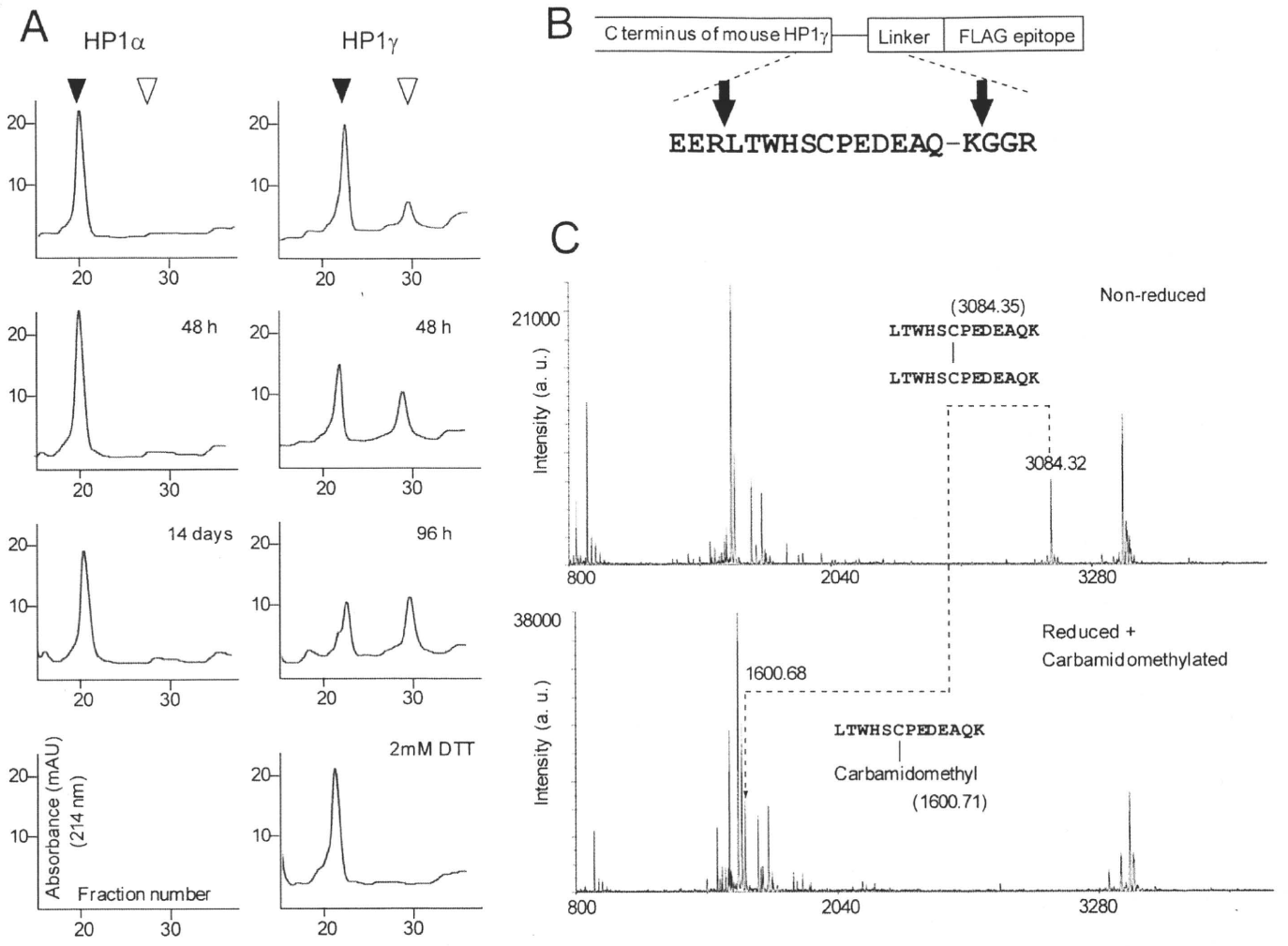

FIGURE 3. **HP1γ is more sensitive to oxidation than HP1α *in vitro*.** MALDI-TOF/MS analysis confirms the disulfide bond formation of HP1γ via Cys-177. *A*, HP1α-FLAG or HP1γ-FLAG expressed in COS7 cells was purified by an anion-exchange column and further fractionated by reverse-phase HPLC. The HPLC absorption pattern profiles at 214 nm are shown. *Black* or *white arrowheads* indicate the fraction of hydrophilic (monomer) or hydrophobic (dimer) forms of HP1, respectively. HP1α-FLAG was fractionated by reverse-phase HPLC immediately after anion exchange (*left top*) or after air oxidation at 4 °C for 48 h or 14 days. HP1γ-FLAG was fractionated immediately after anion exchange (*right top*) or after air oxidation at 4 °C for 48 or 96 h. The HP1γ-FLAG oxidized for 6 days was incubated with 2 mM DTT at 4 °C for 1 h and fractionated by reverse-phase HPLC (*right bottom*). *B*, C-terminal structure of HP1γ-FLAG. *Arrowheads* indicate the trypsin digestion positions. *C*, mass spectra from MALDI-TOF/MS analysis of nonreduced (*upper panel*) or reduced, carbamidomethylated (*lower panel*) HP1γ-FLAG. The expected sequence and estimated mass (*m/z*) of the digested peptide are shown.

was rapidly formed within minutes and was only formed via Cys-177 (Fig. 4*C*). The I165E mutation, which inhibits both noncovalent α-helix dimer formation and proper nuclear localization (6–7), decreased, but not completely, the amount of disulfide dimers of HP1γ (supplemental Fig. S3*A*). These data suggest that the oxidative dimerization of HP1γ requires the proper localization and formation of constitutive, noncovalent dimers.

In contrast to HP1γ, an increase in dimerized HP1α was not observed under the same *in vivo* oxidative conditions (Fig. 4*B*, *right panel*). The dimerized forms of HP1α and HP1γ under basal conditions were almost undetectable without using the large scale purification shown in Fig. 1 because of their relatively low abundance before oxidant treatment. Menadione treatment promoted HP1γ dimerization in various cells, but the extent of dimerization varied among cell types (supplemental Fig. S3*B*), suggesting that the reactivity of HP1γ to reactive oxygen species stimulation varied according to cell type. In each cell, an increase in dimerized HP1α was not observed (data not shown). These results demonstrate that there is a clear difference in oxidation sensitivity among HP1 family members. Although both HP1α and HP1γ have oxidation-sensitive cysteines in their sequences, HP1γ perceives oxidative conditions and is able to more readily form a disulfide dimer than HP1α.

In HEK293T cells, the dimerized HP1γ was subsequently reduced to the monomer form after removal of the oxidant (Fig. 4*D*, *upper panel*), but HP1γ remained dimerized when continuously exposed to the oxidants (Fig. 4*D*, *lower panel*), suggesting that this oxidative modification was reversible.

H_2O_2, known as an endogenous source of reactive oxygen species, also promoted dimerization of HP1γ (Fig. 4*E*). This effect of H_2O_2 was relatively weak in HEK293T cells when compared with the treatment of menadione. However, the same concentration of H_2O_2 substantially increased the amount of dimerized HP1γ in HUVECs (Fig. 4*E*, *lower panel*). Therefore, we further examined the molecular characteristics of the disulfide dimerization of HP1γ using HUVECs.

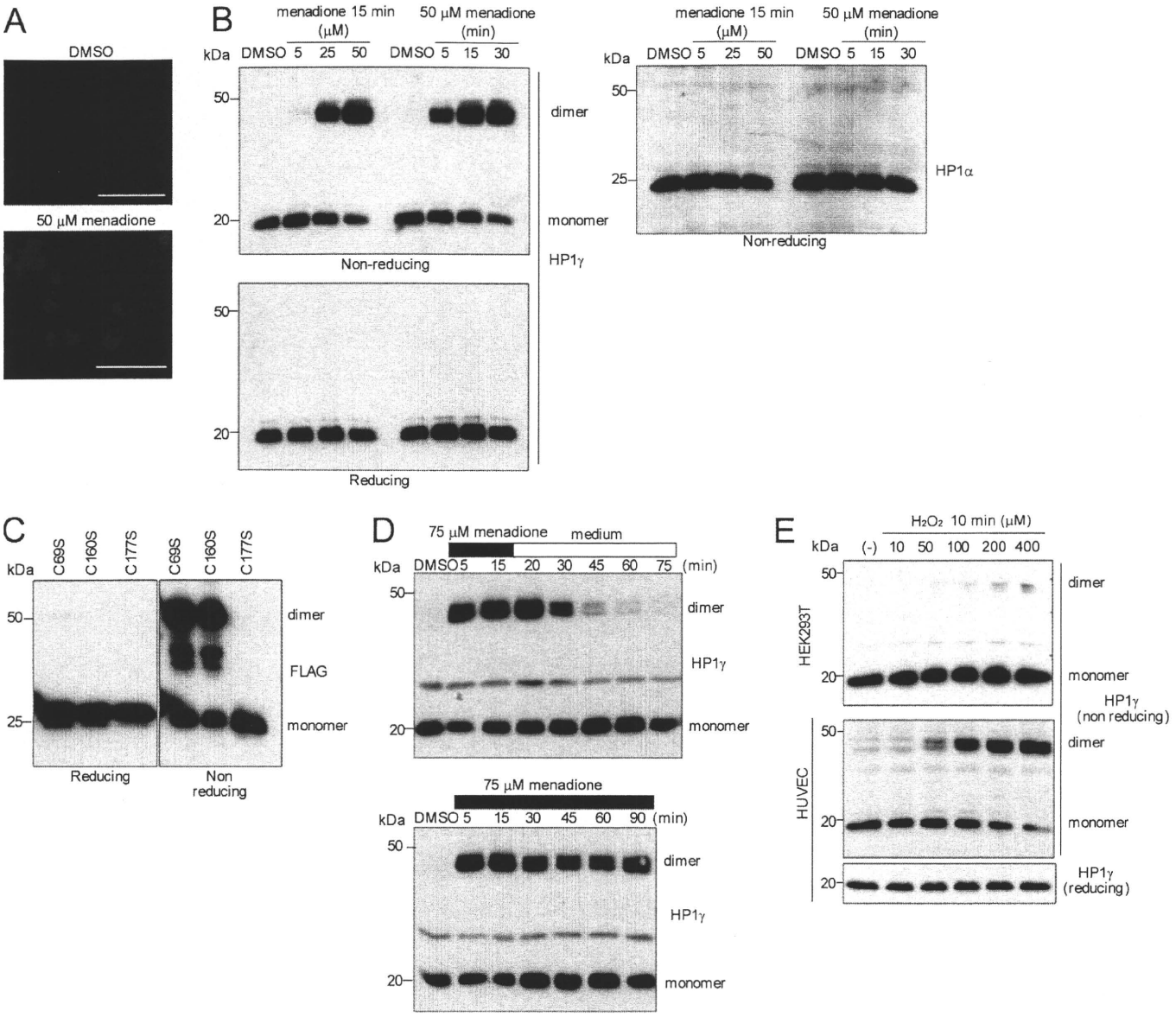

FIGURE 4. **HP1γ, but not HP1α, readily forms disulfide bonds under oxidative conditions.** *A*, after treatment with DMSO or 50 μM menadione for 15 min, COS7 cells were stained with 20 μM dihydroethidium for 30 min and monitored by fluorescence microscopy. *Bar*, 100 μm. *B*, COS7 cells treated with DMSO or menadione under the indicated conditions were lysed, resolved by nonreducing (*upper panel*) or reducing (*lower panel*) SDS-PAGE, and probed with anti-HP1γ antibody. The same membrane was reprobed with anti-HP1α antibody (*right panel*). *C*, COS7 cells expressing each cysteine-to-serine mutant HP1γ-FLAG were treated with 50 μM menadione for 15 min. Lysates were resolved by reducing (*left panel*) or nonreducing (*right panel*) SDS-PAGE and probed with anti-FLAG antibody. *D*, HEK293T cells were treated with 75 μM menadione for 15 min. Subsequently, the culture medium was exchanged for fresh medium (*upper panel*) or kept unchanged (*lower panel*). After incubation for the indicated time, cell lysates were resolved by nonreducing SDS-PAGE and probed with anti-HP1γ antibody. *E*, HEK293T cells and HUVECs were treated with H_2O_2 under the indicated conditions. Cell lysates were resolved by SDS-PAGE and probed with anti-HP1γ antibody. *B–E*, cells were lysed with a buffer (10 mM Tris-HCl, pH 7.2, 150 mM NaCl, 1 mM EDTA, and 1% Nonidet P-40) containing 100 mM maleimide, a thiol-alkylating agent, to prevent artifactual oxidation.

Under Oxidative Conditions, HP1γ Strongly and Transiently Interacts with TIF1β and Holds It in a Chromatin Component—The CSD of HP1, which includes Cys-177 at its C terminus, creates a binding surface for other proteins (27). Therefore, disulfide modification of HP1γ may affect the interactions between HP1 and HP1-binding proteins. Because many candidate effectors that bind to HP1 exist (8), we screened the interacting proteins of HP1γ under oxidative conditions using metabolically radiolabeled HUVECs expressing recombinant HP1γ-FLAG transduced with adenovirus. Among the co-immunoprecipitated proteins, one protein band was detected after treatment with H_2O_2 (Fig. 5*A*, *arrowhead*). The bound protein was purified and analyzed by MALDI-TOF/MS. The amino acid sequence of the digested peptides corresponded to TIF1β (also known as TRIM28 or KAP1), which is a universal co-repressor of gene transcription and is a well known interacting partner of HP1 (28–31). Co-immunoprecipitation analysis showed that endogenous HP1γ strongly interacted with TIF1β in a dose-dependent manner after H_2O_2 treatment (Fig. 5*B*). TIF1β did not interact with HP1γ with a C177S mutation under oxidative conditions, suggesting that the disulfide bond formation of HP1γ enhanced the interaction of these proteins (Fig. 5*C*). When the oxidant was removed, TIF1β dissociated again from HP1γ, suggesting that this enhanced endogenous interac-

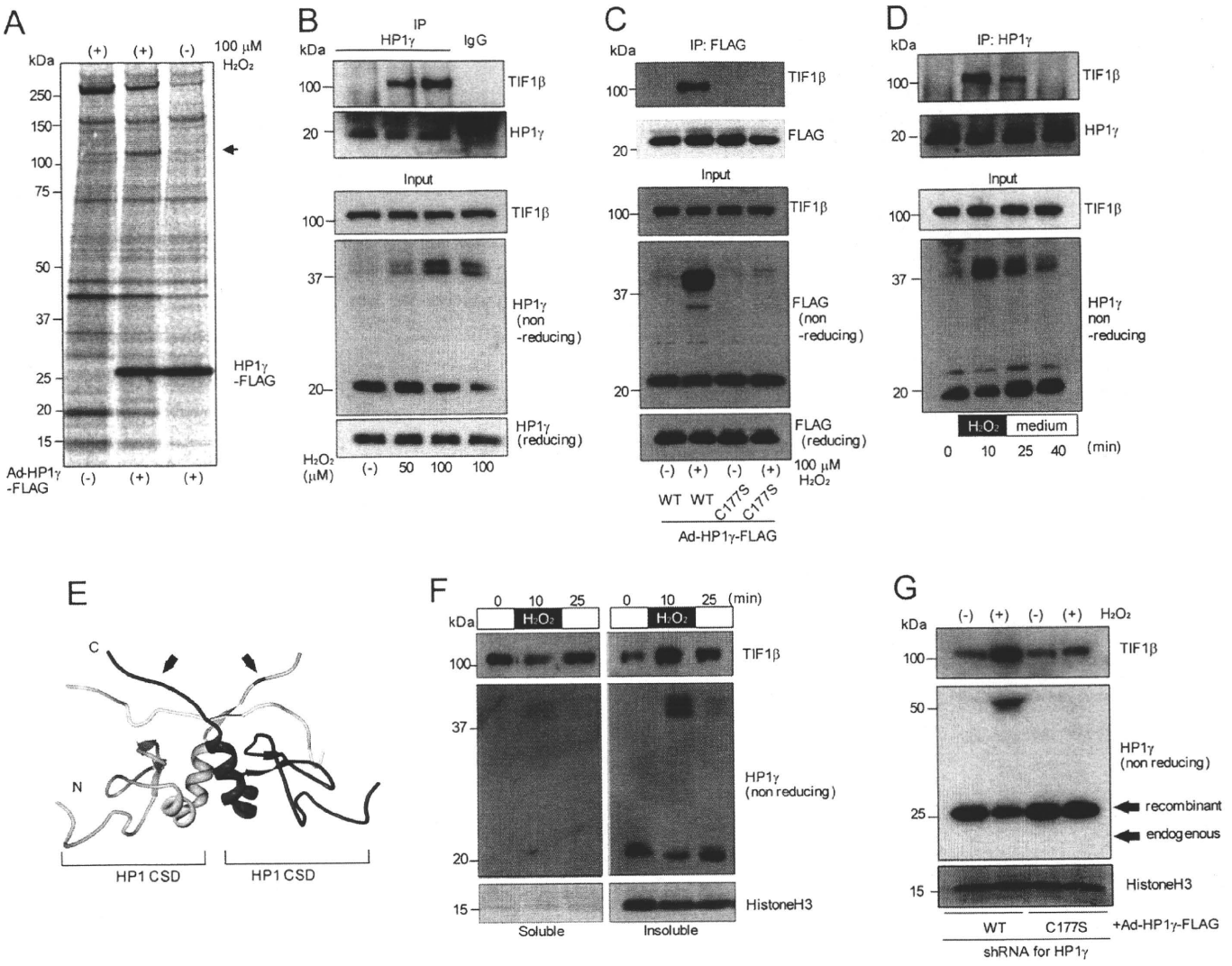

FIGURE 5. **HP1γ strongly interacts with TIF1β and promotes translocation of TIF1β to a chromatin component when dimerized under oxidative conditions.** *A*, HUVECs expressing HP1γ-FLAG (transduced by adenovirus) were metabolically labeled with [^{35}S]cysteine and -methionine for 6 h. Nontransduced cells were also labeled as a negative control. Forty eight h after transduction, the cells were treated with 100 μM H_2O_2 or control (water) for 10 min, lysed, and immunoprecipitated with anti-FLAG M2 affinity gel. Bound samples were resolved by reducing SDS-PAGE and visualized by autoradiography. The *arrow* indicates the protein band co-immunoprecipitated with HP1γ-FLAG only under the oxidative conditions. *B*, lysates from HUVECs treated with control (water) or H_2O_2 for 10 min were immunoprecipitated (*IP*) with anti-HP1γ antibody. Bound samples were resolved by SDS-PAGE and probed with the indicated antibodies. *C*, HUVECs expressing WT or C177S HP1γ-FLAG (transduced by adenovirus) were treated with 100 μM H_2O_2 for 10 min. Lysates were immunoprecipitated with anti-FLAG M2 affinity gel, and bound samples were resolved by SDS-PAGE and probed with the indicated antibodies. *D*, HUVECs were transiently treated with 100 μM H_2O_2. Lysates were immunoprecipitated with anti-HP1γ antibody, and bound samples were resolved by SDS-PAGE and probed with the indicated antibodies. *E*, structure of HP1 CSD noncovalent homodimer (*blue* and *cyan*) and PXVXL motif (*yellow*) complex (Protein Data Bank code 1s4z, modified using the WEB tool (43)). The position of Cys-177 in HP1γ is highlighted in *red* (*black arrows*). *F*, HUVECs were transiently treated with 100 μM H_2O_2. Soluble and insoluble nuclear fractions were obtained using Triton extraction. Each sample was resolved by SDS-PAGE and probed with the indicated antibodies. *G*, HUVECs were transduced with lentivirus expressing shRNA against HP1γ and adenovirus expressing shRNA-resistant HP1γ-FLAG WT or C177S mutant. Triton-insoluble fractions from these cells after H_2O_2 treatment were resolved by SDS-PAGE and probed with the indicated antibodies.

tion was transient (Fig. 5*D*). Structurally, disulfide dimerization via Cys-177 is formed at the C terminus of the CSD, just adjacent to the binding interface for the PXVXL motif, which is a well characterized binding sequence in HP1-interacting proteins, including TIF1β (Fig. 5*E*) (7).

We next examined the localization changes of these proteins before and after oxidant treatment. No remarkable change in localization was detected by immunostaining (data not shown). However, biochemical analysis using Triton extraction verified the TIF1β translocation. HP1γ existed mainly in the Triton-insoluble chromatin component, whereas TIF1β was distributed both in the soluble and the insoluble components (Fig. 5*F*). Under oxidative conditions, HP1γ dimerized and was maintained in the insoluble components. Concomitant with HP1γ dimerization, the insoluble component of TIF1β transiently increased. The knockdown of endogenous HP1γ combined with the replacement by a C177S mutant of HP1γ inhibited the translocation of TIF1β, suggesting that HP1γ held TIF1β on chromatin only when oxidized via Cys-177 (Fig. 5*G*). These data suggest that the intracellular redox state is transduced to the conformational and localization change of the repressor complex via oxidative modification of HP1γ.

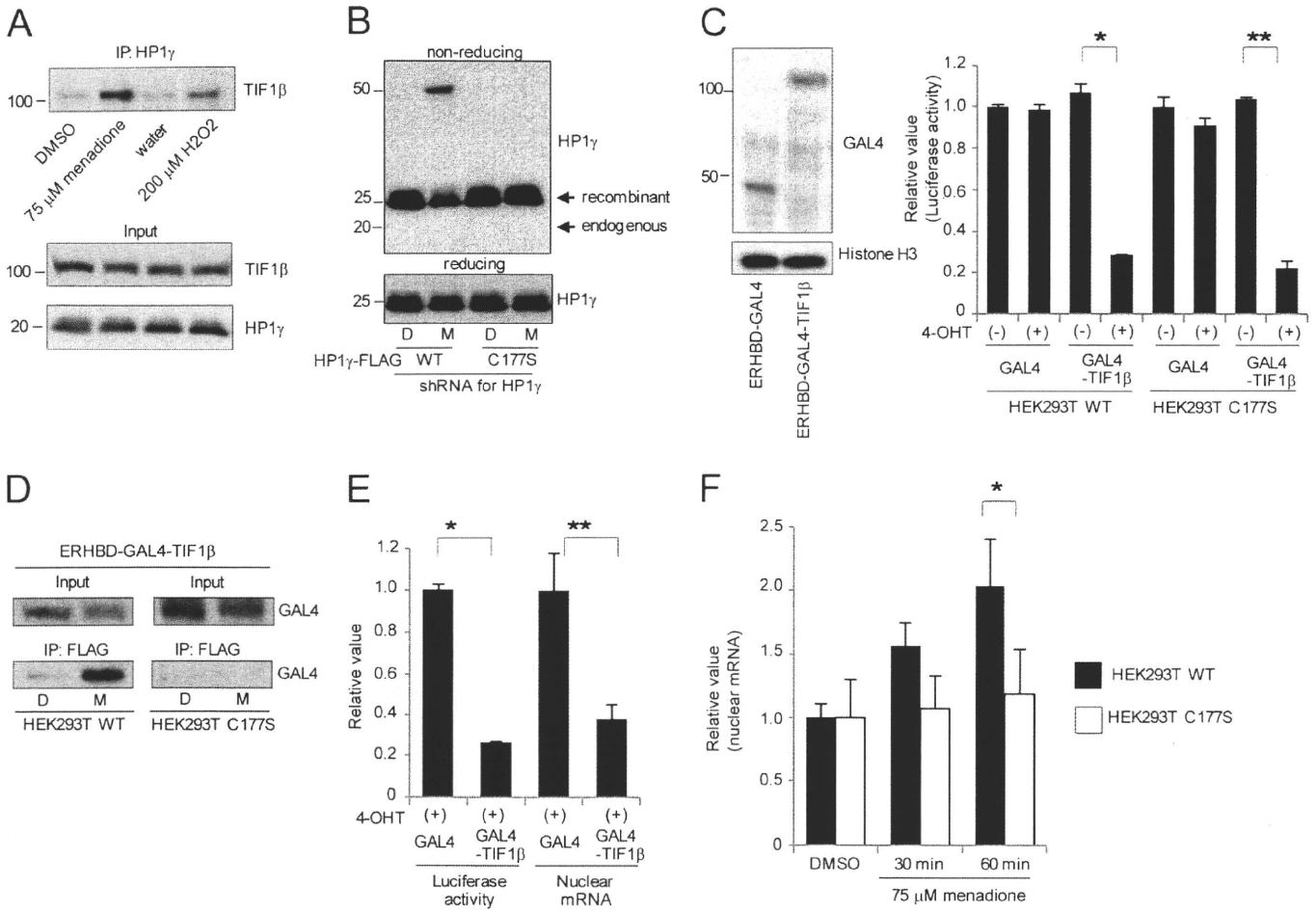

FIGURE 6. **Dimerized HP1γ under oxidative conditions inhibits the repression ability of TIF1β.** *A*, lysates from HEK293T cells treated with DMSO, 75 μM menadione, water, or 200 μM H_2O_2 for 15 min were immunoprecipitated (*IP*) with anti-HP1γ antibody. Bound samples were resolved by SDS-PAGE and probed with the indicated antibodies. *B*, HEK293T cells stably expressing shRNA for HP1γ and shRNA-resistant recombinant FLAG-tagged HP1γ were treated with DMSO or 75 μM menadione for 15 min. Cell lysates were resolved by nonreducing or reducing SDS-PAGE and probed with anti-HP1γ antibody. *D* indicates DMSO, and *M* indicates 75 μM menadione. *C*, lysates from HEK293T stable cells transfected with an ERHBD-GAL4 or ERHBD-GAL4-TIF1β fusion protein were resolved by SDS-PAGE and probed with the indicated antibodies (*left panel*). HEK293T stable cells were transfected with the plasmids encoding ERHBD-GAL4 or ERHBD-GAL4-TIF1β with the reporter plasmids. Twenty four h after transfection, 4-OHT was added to culture medium (500 nM). Forty eight h after transfection, luciferase activity was measured (*right panel*). The relative value was corrected by the value of the cells transfected with ERHBD-GAL4 without 4-OHT induction. Student's *t* test; *, **, $p < 0.01$. *D*, HEK293T stable cells expressing ERHBD-GAL4-TIF1β were treated with DMSO or 75 μM menadione for 15 min. Lysates were immunoprecipitated with anti-FLAG affinity gel. Bound samples were immunoblotted with anti-GAL4 antibody. *D* indicates DMSO, and *M* indicates 75 μM menadione. *E*, under the same conditions as *C*, luciferase transcription levels were determined both by protein enzymatic activity and intranuclear mRNA levels measured by quantitative PCR. Student's *t* test; *, **, $p < 0.01$. *F*, HEK293T stable cells expressing ERHBD-GAL4-TIF1β with 500 nM 4-OHT induction were treated with DMSO for 60 min or 75 μM menadione for the indicated time. Intranuclear luciferase mRNA levels at each time point were measured by quantitative PCR. The relative value was corrected by the value of the cells treated with DMSO. Two-way repeated measure analysis of variance; *, $p < 0.05$. The means ± S.D. as indicated by the *error bars* were determined from three independent experiments.

Dimerized HP1γ under Oxidative Conditions Inhibits the Repression Ability of TIF1β—To clarify whether the repression ability of TIF1β was promoted or inhibited when trapped by HP1γ under oxidative conditions, we used a GAL4-based transcriptional reporter assay. In HEK293T cells, menadione treatment promoted the disulfide dimerization of HP1γ and the interaction between HP1γ and TIF1β more prominently than H_2O_2 treatment (supplemental Fig. S3*B* and Figs. 4*E* and 6*A*). Therefore, we used menadione treatment for further analysis in HEK293T cells. We generated HEK293T cells stably expressing shRNA for HP1γ and shRNA-resistant recombinant FLAG-tagged HP1γ WT or C177S mutant. In these cells, endogenous HP1γ was almost completely depleted and was replaced by the dimerizable or undimerizable recombinant proteins (Fig. 6*B*). To evaluate the transcriptional repression ability of TIF1β, we transfected the plasmids encoding ERHBD-GAL4 as a control or ERHBD-GAL4-TIF1β fusion protein with the reporter plasmids in these cells (12, 32). The transcriptional regulatory activity of the ERHBD fusion protein is post-translationally controlled by the addition of 4-OHT to the culture medium (12). In our experimental conditions where ERHBD-GAL4 and ERHBD-GAL4-TIF1β were equally expressed (Fig. 6*C*, *left panel*), only ERHBD-GAL4-TIF1β repressed transcription of luciferase with 4-OHT (500 nM) in the HEK293T stable cells (Fig. 6*C*, *right panel*). The extent of repression was similar between the cells expressing either the HP1γ-FLAG WT or the C177S mutant under nonoxidative conditions. When the cells were treated with menadione, HP1γ-FLAG WT strongly interacted with ERHBD-GAL4-TIF1β as was similarly observed with endogenous proteins (Fig. 6*D*). To examine the transcrip-

tional change of the luciferase gene under oxidative conditions, we measured the intranuclear mRNA levels of luciferase by quantitative PCR instead of luciferase protein enzymatic activity (Fig. 6*E*). We chose this end point because the oxidation of HP1γ was too rapid to properly evaluate its effect on luciferase transcription by measuring luciferase protein enzymatic activity. Under these conditions, menadione treatment relieved the levels of luciferase transcription repressed by ERHBD-GAL4-TIF1β in the cells expressing HP1γ-FLAG WT but did not relieve the levels in the cells expressing the C177S mutant (Fig. 6*F*). These data suggest that dimerized HP1γ under oxidative conditions inhibits the repression ability of TIF1β.

It remained unclear whether the intranuclear redox-sensing mechanism through the oxidative modification of HP1γ plays a role in the cellular response to extrinsic oxidative stress. Therefore, we assessed the effect of this modification on cell survival under oxidative conditions using HEK293T cells stably expressing shRNA against HP1γ (supplemental Fig. S4*A*). Depletion of HP1γ using shRNA uniformly decreased cell viability under oxidative conditions induced by menadione treatment (supplemental Fig. S4*B*). For a rescue experiment, these stable clones were transduced with an adenoviral vector encoding WT HP1γ-FLAG or C177S HP1γ-FLAG. Both HP1γ vectors were cloned from murine cDNA and were resistant to shRNA against human HP1γ. Transduction of both adenoviral constructs at a multiplicity of infection of 20 resulted in nearly equal expression of recombinant HP1γ with endogenous HP1γ and yielded a similar disulfide dimerization pattern (supplemental Fig. S4*C*). Under these conditions, WT HP1γ-FLAG rescued cell viability after menadione treatment in each stable clone, but the C177S HP1γ-FLAG mutant did not rescue cell viability (supplemental Fig. S4*D*). These results suggest that HP1γ disulfide dimerization plays a pivotal role in cell survival under oxidative conditions.

DISCUSSION

In this study, we identified isoform-specific disulfide bond formation, which is a novel post-translational modification of HP1, using a unique column chromatography method. Biochemical analysis revealed two isoform-specific reactive cysteine residues, cysteine 133 in HP1α and cysteine 177 in HP1γ. In particular, HP1γ readily and reversibly formed disulfide dimers under oxidative conditions. Dimerized HP1γ strongly interacted with TIF1β and held it in a chromatin component. The GAL4 tethering repression assay revealed that the tight interaction of the repressor proteins had a reversing effect for transcriptional repression.

Several post-translational modifications of HP1 have been reported. Specifically, the linker region between the CSD and CD is highly amenable to post-translational modifications, especially phosphorylation that affects silencing activity or nuclear location of HP1 (17, 33–35). Also in the CD, Thr-51 of HP1β has been shown to be phosphorylated in response to DNA damage (22). More recently, a comprehensive proteomic analysis revealed that all HP1 isoforms are highly modified by phosphorylation, acetylation, methylation, and formylation both in the CD and in the CSD (36). Prior to this study, however, no oxidative modification of HP1 had been identified. Because oxidative modifications at cysteine residues would be easily disrupted under reducing conditions, such modifications may be detected only by the unique HPLC-based method used in this study and not by ordinary mass spectrometry analysis.

Both isoform-specific cysteines involved in forming disulfide bonds reside in a structurally flexible region of the CSD. Cys-133 of HP1α lies in the long loop between the β1 and β2 sheets, and Cys-177 of HP1γ lies in the C-terminal region. Introducing cysteine residues into these flexible sites of HP1β conferred the ability to form disulfide bonds, suggesting that these sites have specific structures in the oxidative center. Although both cysteines were reactive, a distinct difference of sensitivity to oxidation existed. Each location of reactive cysteines and the surrounding structure might determine the sensitivity of HP1α and -γ to oxidation. Under both *in vitro* and *in vivo* oxidative conditions, HP1γ readily formed disulfide bonds. In contrast, only minimal disulfide formation of HP1α by oxidation was observed under our experimental conditions. The reactivity of HP1α under oxidation might be observed under different conditions. Nonetheless, the isoform specificity and functional importance of Cys-133 in HP1α has been reported previously (15).

HP1 has been reported to form dimers via the CSD, but these dimers are not mediated by disulfide bonds or other covalent bonds (6, 37, 38). Thus, HP1 dimerizes in at least two ways. The interface of the noncovalently linked dimer involves a symmetrical interaction on helix α2 of the CSD (27) and creates a nonpolar groove structure, which is a binding site for the PXVXL motif in HP1-interacting proteins, such as TIF1β (Fig. 5*E*) (7). Because reactive cysteine 177 in HP1γ is located in the C terminus adjacent to the groove structure, disulfide bond formation at this site likely affects the binding affinity of HP1γ. Indeed, HP1γ strongly and transiently interacted with TIF1β and promoted its translocation to a chromatin component stringently depending on the oxidative status of cysteine 177. This rapid reacting mechanism to transduce cellular redox state to a conformational change like a clear "on-off switch" suggests that HP1γ is a functional redox sensor.

During the cellular response to oxidative stress, an increase in oxidants can trigger alterations in transcription levels through direct activation or by promoting a change in the subcellular localization of transcription factors by oxidizing reactive cysteine residues (25). Among these oxidative responses, the disulfide dimerization of HP1γ demonstrated in this study appears to be one of the most rapid transcriptional regulatory mechanisms. TIF1β is a universal co-repressor for the Krüppel-associated box domain containing the zinc finger protein (KRAB-ZNF) family of transcription factors, and it is the major protein binding the CSD of HP1 (28–31). TIF1β also works as a scaffold for the repressor complex, and its interaction with HP1 is essential for its repression activity (12, 39–41). Recent findings have revealed that the binding of HP1 to TIF1β is essential for their coordinated function on the promoter of the endogenous genes (42). Therefore, the reversing effect for the repressive ability of TIF1β caused by HP1γ disulfide dimerization might be required for a short period of adaptation against oxidative stress. Downstream genes regulated by these scaffold complexes remain to be clarified in the future analysis.

In conclusion, our study suggests that HP1 potentially acts as a rapid redox sensor, and it may connect the intracellular redox state with transcriptional regulation under various physiological conditions.

Acknowledgments—We thank David C. Schultz and Takahiro Nagase for the plasmid constructs. We thank Saori Ikezawa and Yoko Hamada for technical assistance and Yasunori Shintani for thoughtful discussions.

REFERENCES

1. James, T. C., and Elgin, S. C. (1986) *Mol. Cell. Biol.* **6,** 3862–3872
2. Wallrath, L. L. (1998) *Curr. Opin. Genet. Dev.* **8,** 147–153
3. Bannister, A. J., Zegerman, P., Partridge, J. F., Miska, E. A., Thomas, J. O., Allshire, R. C., and Kouzarides, T. (2001) *Nature* **410,** 120–124
4. Nakayama, J., Rice, J. C., Strahl, B. D., Allis, C. D., and Grewal, S. I. (2001) *Science* **292,** 110–113
5. Lachner, M., O'Carroll, D., Rea, S., Mechtler, K., and Jenuwein, T. (2001) *Nature* **410,** 116–120
6. Brasher, S. V., Smith, B. O., Fogh, R. H., Nietlispach, D., Thiru, A., Nielsen, P. R., Broadhurst, R. W., Ball, L. J., Murzina, N. V., and Laue, E. D. (2000) *EMBO J.* **19,** 1587–1597
7. Thiru, A., Nietlispach, D., Mott, H. R., Okuwaki, M., Lyon, D., Nielsen, P. R., Hirshberg, M., Verreault, A., Murzina, N. V., and Laue, E. D. (2004) *EMBO J.* **23,** 489–499
8. Grewal, S. I., and Jia, S. (2007) *Nat. Rev. Genet.* **8,** 35–46
9. Lomberk, G., Wallrath, L., and Urrutia, R. (2006) *Genome Biol.* **7,** 228
10. Schultz, D. C., Ayyanathan, K., Negorev, D., Maul, G. G., and Rauscher, F. J., 3rd. (2002) *Genes Dev.* **16,** 919–932
11. Maison, C., and Almouzni, G. (2004) *Nat. Rev. Mol. Cell Biol.* **5,** 296–304
12. Sripathy, S. P., Stevens, J., and Schultz, D. C. (2006) *Mol. Cell. Biol.* **26,** 8623–8638
13. Cammas, F., Janoshazi, A., Lerouge, T., and Losson, R. (2007) *Differentiation* **75,** 627–637
14. Filesi, I., Cardinale, A., van der Sar, S., Cowell, I. G., Singh, P. B., and Biocca, S. (2002) *J. Cell Sci.* **115,** 1803–1813
15. Nielsen, A. L., Sanchez, C., Ichinose, H., Cerviño, M., Lerouge, T., Chambon, P., and Losson, R. (2002) *EMBO J.* **21,** 5797–5806
16. Vassallo, M. F., and Tanese, N. (2002) *Proc. Natl. Acad. Sci. U.S.A.* **99,** 5919–5924
17. Lomberk, G., Bensi, D., Fernandez-Zapico, M. E., and Urrutia, R. (2006) *Nat. Cell Biol.* **8,** 407–415
18. Gilbert, N., Boyle, S., Sutherland, H., de Las Heras, J., Allan, J., Jenuwein, T., and Bickmore, W. A. (2003) *EMBO J.* **22,** 5540–5550
19. Ritou, E., Bai, M., and Georgatos, S. D. (2007) *J. Cell Sci.* **120,** 3425–3435
20. Mateescu, B., Bourachot, B., Rachez, C., Ogryzko, V., and Muchardt, C. (2008) *EMBO Rep.* **9,** 267–272
21. Vakoc, C. R., Mandat, S. A., Olenchock, B. A., and Blobel, G. A. (2005) *Mol. Cell* **19,** 381–391
22. Ayoub, N., Jeyasekharan, A. D., Bernal, J. A., and Venkitaraman, A. R. (2008) *Nature* **453,** 682–686
23. Petta, T. B., Nakajima, S., Zlatanou, A., Despras, E., Couve-Privat, S., Ishchenko, A., Sarasin, A., Yasui, A., and Kannouche, P. (2008) *EMBO J.* **27,** 2883–2895
24. Asano, Y., Takashima, S., Asakura, M., Shintani, Y., Liao, Y., Minamino, T., Asanuma, H., Sanada, S., Kim, J., Ogai, A., Fukushima, T., Oikawa, Y., Okazaki, Y., Kaneda, Y., Sato, M., Miyazaki, J., Kitamura, S., Tomoike, H., Kitakaze, M., and Hori, M. (2004) *Nat. Genet.* **36,** 123–130
25. D'Autréaux, B., and Toledano, M. B. (2007) *Nat. Rev. Mol. Cell Biol.* **8,** 813–824
26. Oka, S., Ohno, M., Tsuchimoto, D., Sakumi, K., Furuichi, M., and Nakabeppu, Y. (2008) *EMBO J.* **27,** 421–432
27. Cowieson, N. P., Partridge, J. F., Allshire, R. C., and McLaughlin, P. J. (2000) *Curr. Biol.* **10,** 517–525
28. Friedman, J. R., Fredericks, W. J., Jensen, D. E., Speicher, D. W., Huang, X. P., Neilson, E. G., and Rauscher, F. J., 3rd. (1996) *Genes Dev.* **10,** 2067–2078
29. Kim, S. S., Chen, Y. M., O'Leary, E., Witzgall, R., Vidal, M., and Bonventre, J. V. (1996) *Proc. Natl. Acad. Sci. U.S.A.* **93,** 15299–15304
30. Le Douarin, B., Nielsen, A. L., Garnier, J. M., Ichinose, H., Jeanmougin, F., Losson, R., and Chambon, P. (1996) *EMBO J.* **15,** 6701–6715
31. Moosmann, P., Georgiev, O., Le Douarin, B., Bourquin, J. P., and Schaffner, W. (1996) *Nucleic Acids Res.* **24,** 4859–4867
32. Itokawa, Y., Yanagawa, T., Yamakawa, H., Watanabe, N., Koga, H., and Nagase, T. (2009) *Biochem. Biophys. Res. Commun.* **388,** 689–694
33. Koike, N., Maita, H., Taira, T., Ariga, H., and Iguchi-Ariga, S. M. (2000) *FEBS Lett.* **467,** 17–21
34. Zhao, T., Heyduk, T., and Eissenberg, J. C. (2001) *J. Biol. Chem.* **276,** 9512–9518
35. Badugu, R., Yoo, Y., Singh, P. B., and Kellum, R. (2005) *Chromosoma* **113,** 370–384
36. Leroy, G., Weston, J. T., Zee, B. M., Young, N. L., Plazas-Mayorca, M. D., and Garcia, B. A. (2009) *Mol. Cell. Proteomics* **8,** 2432–2442
37. Wang, G., Ma, A., Chow, C. M., Horsley, D., Brown, N. R., Cowell, I. G., and Singh, P. B. (2000) *Mol. Cell. Biol.* **20,** 6970–6983
38. Nielsen, A. L., Oulad-Abdelghani, M., Ortiz, J. A., Remboutsika, E., Chambon, P., and Losson, R. (2001) *Mol. Cell* **7,** 729–739
39. Nielsen, A. L., Ortiz, J. A., You, J., Oulad-Abdelghani, M., Khechumian, R., Gansmuller, A., Chambon, P., and Losson, R. (1999) *EMBO J.* **18,** 6385–6395
40. Ayyanathan, K., Lechner, M. S., Bell, P., Maul, G. G., Schultz, D. C., Yamada, Y., Tanaka, K., Torigoe, K., and Rauscher, F. J., 3rd. (2003) *Genes Dev.* **17,** 1855–1869
41. Smallwood, A., Black, J. C., Tanese, N., Pradhan, S., and Carey, M. (2008) *Nat. Struct. Mol. Biol.* **15,** 318–320
42. Riclet, R., Chendeb, M., Vonesch, J. L., Koczan, D., Thiesen, H. J., Losson, R., and Cammas, F. (2009) *Mol. Biol. Cell* **20,** 296–305
43. Moreland, J. L., Gramada, A., Buzko, O. V., Zhang, Q., and Bourne, P. E. (2005) *BMC Bioinformatics* **6,** 21

This Review is part of a thematic series on **Endoplasmic Reticulum Stress and Cardiac Diseases**, which includes the following articles:
What Is the Role of ER Stress in the Heart? Introduction and Series Overview [*Circ Res.* 2010;107:15–18]
The Role of Endoplasmic Reticulum Stress in the Progression of Atherosclerosis [*Circ Res.* 2010;107:839–850]

Endoplasmic Reticulum Stress As a Therapeutic Target in Cardiovascular Disease

Biology of Endoplasmic Reticulum Stress in the Heart
Interrelationship Between Cardiac Hypertrophy, Heart Failure, and Chronic Kidney Disease—Endoplasmic Reticulum

Masafumi Kitakaze, Guest Editor

Endoplasmic Reticulum Stress As a Therapeutic Target in Cardiovascular Disease

Tetsuo Minamino, Issei Komuro, Masafumi Kitakaze

Abstract: **Cardiovascular disease constitutes a major and increasing health burden in developed countries. Although treatments have progressed, the development of novel treatments for patients with cardiovascular diseases remains a major research goal. The endoplasmic reticulum (ER) is the cellular organelle in which protein folding, calcium homeostasis, and lipid biosynthesis occur. Stimuli such as oxidative stress, ischemic insult, disturbances in calcium homeostasis, and enhanced expression of normal and/or folding-defective proteins lead to the accumulation of unfolded proteins, a condition referred to as ER stress. ER stress triggers the unfolded protein response (UPR) to maintain ER homeostasis. The UPR involves a group of signal transduction pathways that ameliorate the accumulation of unfolded protein by increasing ER-resident chaperones, inhibiting protein translation and accelerating the degradation of unfolded proteins. The UPR is initially an adaptive response but, if unresolved, can lead to apoptotic cell death. Thus, the ER is now recognized as an important organelle in deciding cell life and death. There is compelling evidence that the adaptive and proapoptotic pathways of UPR play fundamental roles in the development and progression of cardiovascular diseases, including heart failure, ischemic heart diseases, and atherosclerosis. Thus, therapeutic interventions that target molecules of the UPR component and reduce ER stress will be promising strategies to treat cardiovascular diseases. In this review, we summarize the recent progress in understanding UPR signaling in cardiovascular disease and its related therapeutic potential. Future studies may clarify the most promising molecules to be investigated as targets for cardiovascular diseases. (*Circ Res.* 2010;107:1071-1082.)**

Key Words: heart failure ■ ischemic heart diseases ■ atherosclerosis ■ ER stress ■ unfolded protein response

Although the clinical management of heart failure has advanced substantially,[1] and prevention strategies for atherosclerosis focused on managing the established risk factors have progressed markedly,[2] cardiovascular disease still constitutes a major and increasing health burden in developed countries. Thus, the development of novel treatments for patients with cardiovascular diseases remains a major research priority.

The endoplasmic reticulum (ER) comprises a complex membranous network found in all eukaryotic cells. It plays a crucial role in the folding of secretory and membrane proteins, calcium homeostasis, and lipid biosynthesis.[3–5] ER

Original received July 6, 2010; revision received September 10, 2010; accepted September 14, 2010. In August 2010, the average time from submission to first decision for all original research papers submitted to *Circulation Research* was 13.2 days.

From the Department of Cardiovascular Medicine (T.M., I.K.), Osaka University Graduate School of Medicine; and Department of Cardiovascular Medicine (M.K.), National Cerebral and Cardiovascular Center Hospital, Japan.

This manuscript was sent to Ali J. Marian, Consulting Editor, for review by expert referees, editorial decision, and final disposition.

Correspondence to Tetsuo Minamino, MD, PhD, Department of Cardiovascular Medicine, Osaka University Graduate School of Medicine, 2-2 Yamadaoka, Suita, Osaka 565-0871, Japan. E-mail minamino@cardiology.med.osaka-u.ac.jp

Circulation Research **is available at http://circres.ahajournals.org** **DOI: 10.1161/CIRCRESAHA.110.227819**

Non-standard Abbreviations and Acronyms

AMPK	AMP-activated protein kinase
ASK1	apoptosis signal-regulating kinase 1
ATF	activating transcription factor
Bcl-2	B-cell lymphoma 2
CHOP	CCAAT/enhancer binding protein (C/EBP) homologous protein
CREBH	cAMP response element-binding protein H
eIF2α	eukaryotic initiation factor-2α
ER	endoplasmic reticulum
ERAD	endoplasmic reticulum–associated degradation
ERO1	endoplasmic reticulum oxidoreductin 1
GRP78	glucose-regulated protein 78 kDa
IκB	inhibitor of κB
I/R	ischemia/reperfusion
IRE1	inositol-requiring protein 1
JNK	c-Jun N-terminal kinase
KO	knockout
MANF	mesencephalic astrocyte-derived neurotrophic factor
PARM-1	prostatic androgen repressed message-1
PBA	phenylbutyrate
PDI	protein disulfide isomerase
PERK	protein kinase–like endoplasmic reticulum kinase
PKA	protein kinase A
ROS	reactive oxygen species
SERCA	sarcoplasmic reticulum calcium-transporting ATPase
TNF	tumor necrosis factor
TRAF2	tumor necrosis factor receptor–associated factor 2
TRB3	tribbles 3
TLR	Toll-like receptor
UPR	unfolded protein response
XBP1	X box–binding protein-1

stress that disrupts ER function can occur in response to a wide variety of cellular stressors that lead to the accumulation of unfolded and misfolded proteins in the ER. Initially, ER transmembrane sensors detect the accumulation of unfolded proteins and activate transcriptional and translational pathways that deal with unfolded and misfolded proteins, known as the unfolded protein response (UPR). However, the failure to relieve prolonged or severe ER stress causes the cell to undergo apoptotic cell death. Recently, adaptive and proapoptotic pathways of UPR have been implicated in the pathophysiology of human diseases, including cardiovascular diseases, neurodegenerative diseases, diabetes mellitus, obesity, and liver diseases.[3–5] In this review, we summarize the molecular mechanisms of UPR in cardiovascular diseases and possible therapeutic interventions targeting the components involved in the UPR.

Endoplasmic Reticulum

The ER is the cellular organelle for the synthesis and folding of secreted and membrane-bound proteins and the first site of the secretory pathway.[3–5] Approximately one-third of newly synthesized proteins are translocated into the ER, where they fold and assemble with the assistance of ER chaperones and oxidoreductases.[6] The ER lumen constitutes a specialized environment for proper protein folding and assembly.[3–5] For instance, the ER contains the millimolar concentrations of free calcium within the cell. Glucose-regulated protein 78 kDa (GRP78), which is the ER-located member of the family of heat shock protein 70 molecular chaperones, promotes the folding of hydrophobic regions in polypeptides to the interior in a calcium-dependent manner.[7] The oxidizing environment in the ER is crucial for the formation of disulfide bonds mediated by protein disulfide isomerase (PDI) and ER oxidoreductin (ERO)1, which serves as the terminal electron acceptor with oxygen.[8] Reactive oxygen species (ROS) generated as a product of disulfide bond formation in the ER cause oxidative stress and contribute to apoptotic cell death.[9] As a consequence of this special environment, the ER is highly sensitive to stresses that deplete its ATP or calcium and alter the intraluminal redox status.

Adaptive and Proapoptotic Pathways of UPR

When unfolded proteins accumulate in the ER, 3 ER transmembrane sensors detect them to initiate 3 distinct UPR branches mediated by the following molecules: protein kinase-like ER kinase (PERK), the inositol requiring kinase (IRE)1, and the transcription factor-activating transcription factor (ATF)6 (Figure 1).[3–5,10] These UPR sensors have N termini in the lumen of the ER and C termini in the cytosol, thereby connecting the ER and cytosol. All 3 sensors have luminal domains that bind to the ER chaperone GRP78 under normal, unstressed conditions.[11] However, on ER stress, GRP78 is released from these sensors, permitting their oligomerization and thereby initiating the UPR to deal with accumulated unfolded proteins. However, if the ER stress is prolonged and/or severe, the ER initiates apoptotic cell death signaling.[12] ER sensor proteins including PERK and IRE1 are responsible for both the adaptive and the proapoptotic pathways of UPR.[12]

IRE1α is the most fundamental ER stress sensor and is conserved from yeast to humans. On ER stress, the dimerization and autophosphorylation of IRE1 elicit an endoribonuclease activity that specifically cleaves the mRNA encoding the transcription factor X-box binding protein (XBP)1.[3–5] This unconventional splicing reaction is required for the translation of transcriptionally active XBP1. Active (spliced) XBP1 binds to the ER stress response element in the promoters of a wide variety of UPR-target genes whose products help to fold and degrade the proteins.[3–5] Our recent study demonstrated that spliced XBP1 can regulate the expression of brain natriuretic peptide (BNP), a non–UPR-target gene, through a novel AP1/CRE-like element in cardiomyocytes.[13] Interestingly, p85α, the regulatory subunit of phosphatidylinositol 3-kinase (PI3K), was found to interact with XBP1 and increase the nuclear translocation of XBP1.[14] In ob/ob mice, the interaction between them is lost, resulting in a severe defect in both the translocation of XBP1 and the resolution of ER stress.[14] These findings suggest that non-UPR and UPR genes are regulated by spliced XBP1.

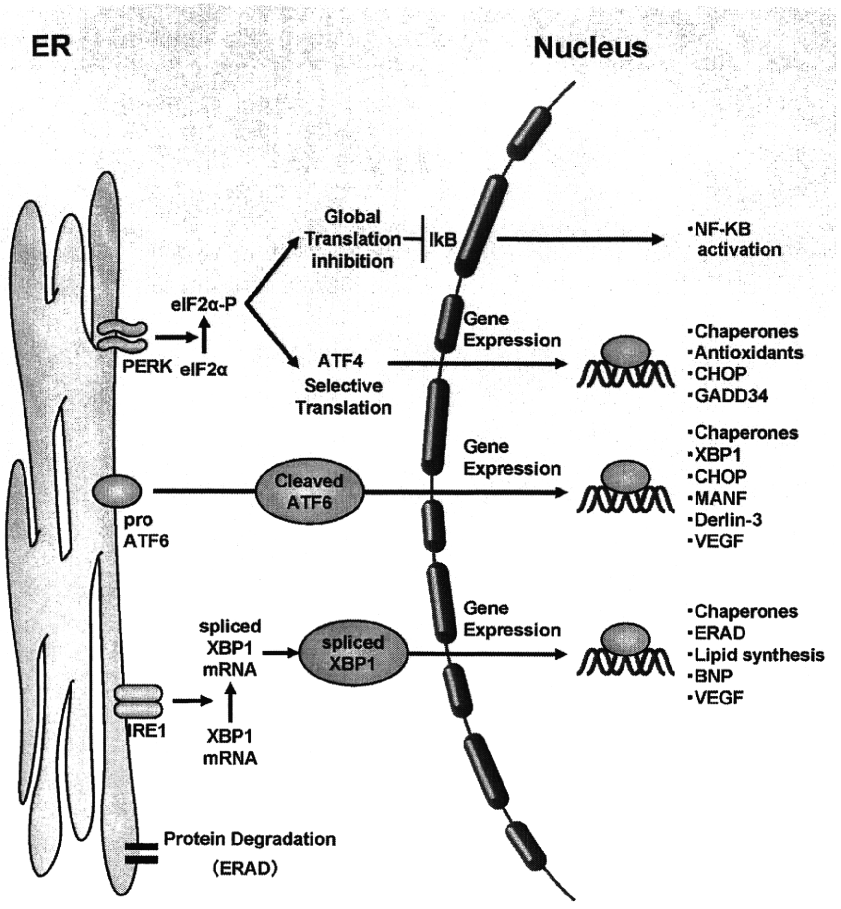

Figure 1. UPR pathways. On ER stress, GRP78 dissociates from 3 ER transmembrane sensors including PERK, IRE1, and ATF6, allowing their activation. PERK phosphorylates eIF2α, which is dephosphorylated by GADD34, consequently shutting off protein translation. However, paradoxically, eIF2α phosphorylation induces the selective translation of a transcriptional factor ATF4 to induce the UPR-target genes. ATF6 translocates from ER to Golgi, in which ATF6 cleavage produces a transcriptionally active cytosolic fragment. ATF6 activates a subset of UPR- and non–UPR-target genes, including XBP1. On ER stress, activation of IRE1 elicits an endoribonuclease activity that specifically cleaves the mRNA encoding the transcriptional factor XBP1. This unconventional splicing reaction is required for translation of transcriptionally active XBP1 to induce UPR- and non–UPR-target genes.

In addition to endoribonuclease activity, IRE1α mediates cell death and inflammatory signaling (Figure 2). IRE1α interacts with the adaptor protein tumor necrosis factor TNF receptor–associated factor (TRAF) 2, which leads to the activation of a mitogen-activated protein kinase kinase kinase, apoptosis signal-regulating kinase (ASK)1[15,16] and caspase 12.[17,18] The ASK1 pathway contributes to the pathogenesis of heart and neurodegenerative diseases.[19,20] Furthermore, IRE1α/TRAF2 can also recruit the inhibitor of κB (IκB) kinase, which mediates the activation of nuclear factor κB, suggesting that IRE1α might provide a link between ER stress and inflammation.[21]

PERK is another ER stress sensor and a serine threonine kinase that phosphorylates eukaryotic translation initiation factor (eIF)2α on ER stress, resulting in the inhibition of most cap-dependent translation, which requires the interaction of certain key molecules with a special tag bound to the 5′-end of mRNA, termed a cap.[3–5] One example is the translational inhibition of IκB, resulting in the activation of nuclear factor κB.[22] However, paradoxically, several mRNAs require the phosphorylation of eIF2α for their translation. One example is the mRNA encoding ATF4, a transcriptional factor that binds to the promoter of the gene encoding GADD34, the regulatory subunit of the phosphatase that dephosphorylates eIF2α and restores cap-dependent translation.[23] CCAAT/enhancer-binding protein homologous protein (CHOP) is the proapoptotic basic-leucine zipper transcription factor that is regulated by the ATF4 and ATF6 pathways.[3–5] The deletion of the CHOP gene protects against cell death induced by a pharmacological ER stressor, mechanical stretching and pathophysiological stimuli, such as ischemia and pressure overload.[24–28] Although the potential mechanisms by which CHOP induces cell death are not well identified, one important pathway by which CHOP induces cell apoptosis is regulation of the balance of proapoptotic and antiapoptotic B-cell lymphoma (Bcl)-2 family proteins. CHOP represses the expression of antiapoptotic proteins Bcl-2 and Bnip3 in cardiomyocytes.[27,29] In addition, CHOP mediates the direct transcriptional induction and translocation to the ER membrane of Bim, a proapoptotic BH3-only protein of the Bcl-2 protein family, in conditions of ER stress.[30]

The third ER stress member is ATF6, a transmembrane basic leucine zipper transcription factor.[3–5] ER stress induces the release of GRP78 from ATF6 and permits ATF6 translocation from the ER to the Golgi, where S1P- and S2P-mediated proteolytic cleavage produces a transcriptionally active cytosolic fragment. Cleaved ATF6 binds to the ER stress response element in the promoters of UPR target genes, including XBP1. Recently, several ATF6-related proteins with distinct tissue distributions were identified.[31,32] Interestingly, lipopolysaccharide and cytokines activate cAMP response element-binding protein (CREB)H, which is a hepatocyte-specific ER-anchored transcription factor that activates a subset of genes associated with inflammation but

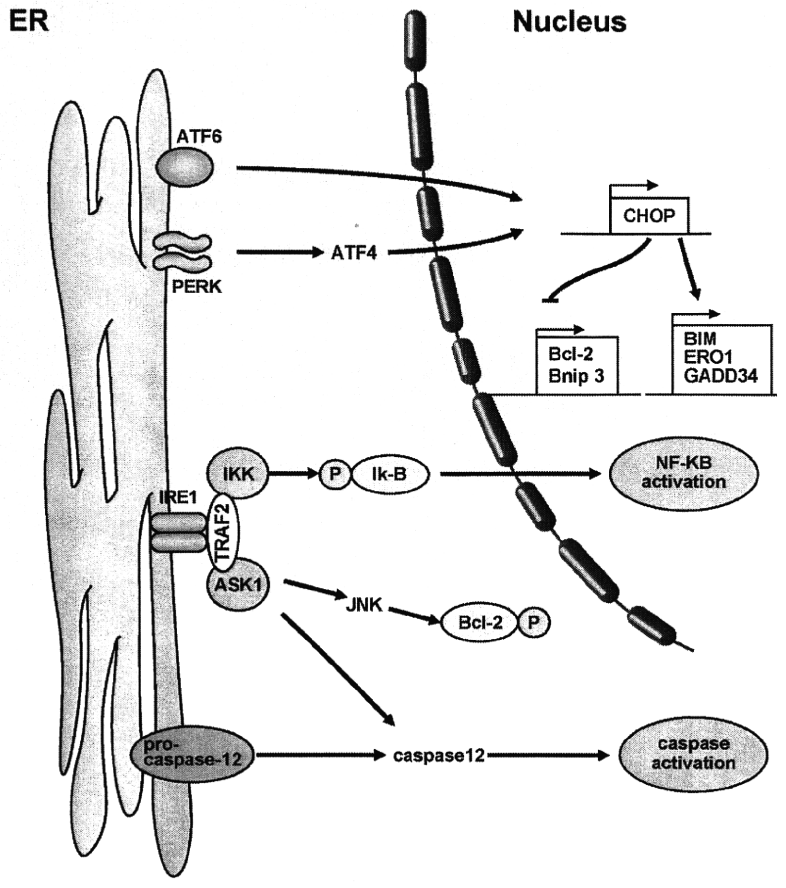

Figure 2. Proapoptotic pathways of UPR. CHOP is the proapoptotic bZIP transcription factor that is regulated mainly by ATF4- and ATF6-dependent pathways. CHOP represses the expression of the antiapoptotic proteins Bcl-2 and Bnip3. In addition, CHOP mediates the direct transcriptional induction and translocation to the ER membrane of Bim, a proapoptotic BH3-only protein of the Bcl-2 family, on ER stress. IRE1α interacts with the adaptor protein TRAF2. The IRE1α/TRAF2 complex interacts with ASK1, which subsequently phosphorylates JNK. Activation of JNK induces apoptotic cell death through the phosphorylation of several Bcl-2 family members. The IRE1α/TRAF2 complex also interacts with IκB kinase, which leads to nuclear factor κB (NF-κB) activation. On ER stress, procaspase 12 is cleaved and activated, which in turn activates caspase-9/3, thereby leading to mitochondria-independent cell death.

not UPR.[31] These findings suggest that CREBH integrates the UPR with the acute phase response. PARM-1 (prostatic androgen repressed message 1) was shown to be induced in a cardiac hypertrophy and subsequent heart failure model.[33] PARM-1 expression is induced by ER stress, which plays a protective role in cardiomyocytes through the regulation of PERK, ATF6 and CHOP expression. The existence of tissue-specific UPR components allows for the response to tissue-specific stress.

Misfolded ER proteins are exported from the ER into the cytosol by a process termed ER-associated protein degradation (ERAD) or retrotranslocation.[3,34] Most ERAD substrates are ubiquitinated and extracted by a cytosolic ATPase named p97 before degradation by the proteasome. Defects in ERAD cause the accumulation of misfolded proteins in the ER and thus trigger the UPR.[35]

ER Stress and Cardiovascular Diseases

Experimentally, the ER environment can be perturbed by substances such as dithiothreitol, thapsigargin, or tunicamycin, which alter the redox status, calcium levels and protein glycosylation in the ER, respectively.[36] When cells are treated with one of these compounds, ER protein folding is impaired, and the accumulation of unfolded proteins activates the adaptive and proapoptotic pathways of the UPR.[3–5]

Pathophysiological stimuli also activate UPR. Hypoxia, angiotensin II and tumor necrosis factor (TNF)-α activate adaptive and proapoptotic pathways of the UPR in cultured cardiomyocytes.[37–39] The cardiac-specific deposition of aggregated β-amyloid[40] or polyglutamine preamyloid oligomer[41] activated the component of UPR in mouse transgenic hearts. Cyclic stretching significantly increases CHOP protein in cultured cardiomyocytes,[28] and CHOP expression increases in pressure-overloaded hearts.[38] Metabolic factors such as cholesterol, homocysteine, glucose, fatty acid, and palmitate can also trigger ER stress.[42,43] These findings suggest that activation of UPR by pathophysiological stimuli is involved in the development of cardiovascular diseases.

Cardiac Hypertrophy and Failure

Electron microscopic analyses have revealed that the proliferation of tubules of the ER is a common finding in degenerated cardiomyocytes, suggesting that the ER is overloaded in this condition.[44] Oxidative stress, hypoxia, and enhanced protein synthesis found in failing hearts potentially enhance ER stress. Indeed, in patients with heart failure, we and others have shown the existence of spliced XBP1 and markedly increased GRP78 expression, suggesting that UPR activation is associated with the pathophysiology of heart failure in humans.[13,38,45] Our study also showed that mRNA levels of ATF4 and CHOP are increased in these patients.[27] Furthermore, ubiquitinated proteins are accumulated in human failing hearts.[46,47] These findings suggest that protein quality control is impaired in human failing hearts.